Theses and Dissertations--Mechanical Engineering

Mechanical Engineering

2018

CHARACTERIZATION OF THE SHAPE MEMORY BEHAVIOR OF HIGH STRENGTH NiTiHfPd SHAPE MEMORY ALLOYS

Guher P. Toker
University of Kentucky, guhertoker@uky.edu
Digital Object Identifier: https://doi.org/10.13023/ETD.2018.133

Click here to let us know how access to this document benefits you.

STUDENT AGREEMENT:

I represent that my thesis or dissertation and abstract are my original work. Proper attribution has been given to all outside sources. I understand that I am solely responsible for obtaining any needed copyright permissions. I have obtained needed written permission statement(s) from the owner(s) of each third-party copyrighted matter to be included in my work, allowing electronic distribution (if such use is not permitted by the fair use doctrine) which will be submitted to UKnowledge as Additional File.

I hereby grant to The University of Kentucky and its agents the irrevocable, non-exclusive, and royalty-free license to archive and make accessible my work in whole or in part in all forms of media, now or hereafter known. I agree that the document mentioned above may be made available immediately for worldwide access unless an embargo applies.

I retain all other ownership rights to the copyright of my work. I also retain the right to use in future works (such as articles or books) all or part of my work. I understand that I am free to register the copyright to my work.

REVIEW, APPROVAL AND ACCEPTANCE

The document mentioned above has been reviewed and accepted by the student's advisor, on behalf of the advisory committee, and by the Director of Graduate Studies (DGS), on behalf of the program; we verify that this is the final, approved version of the student's thesis including all changes required by the advisory committee. The undersigned agree to abide by the statements above.

Guher P. Toker, Student

Dr. Haluk E. Karaca, Major Professor

Dr. Haluk E. Karaca, Director of Graduate Studies

CHARACTERIZATION OF THE SHAPE MEMORY BEHAVIOR OF HIGH STRENGTH NiTiHfPd SHAPE MEMORY ALLOYS

THESIS

A thesis submitted in partial fulfillment of the

requirements for the degree of

Master of Science in Mechanical Engineering

in the College of Engineering

at the University of Kentucky

By

Guher Pelin Toker

Lexington, Kentucky

Director: Dr. Haluk E. Karaca, Professor of Mechanical Engineering

Lexington, Kentucky

2018

ABSTRACT OF THESIS

CHARACTERIZATION OF THE SHAPE MEMORY BEHAVIOR OF HIGH STRENGTH NiTiHfPd SHAPE MEMORY ALLOYS

NiTiHf alloys have emerged as potential materials for applications requiring high transformation temperatures ($> 100\ °C$) with high strength and work output. Although they have high transformation temperatures, their low damping capacity, brittleness and poor superelastic responses (of Ti-rich NiTiHf) impedes their wider usage in many industrial applications. In this study, the quaternary alloying element of Pd has been added to NiTiHf alloys to improve and tailor their shape memory behavior,. NiTiHfPd alloys were systematically examined regarding the composition and heat treatments effects.

Effects of substituting Hf with Ti on the shape memory behavior of NiTHfPd alloys were investigated. There compositions were selected as $Ni_{40.3}Ti_{34}Hf_{20}Pd_5$ $Ni_{40.3}Ti_{39.7}Hf_{15}Pd_5$ and $Ni_{40.3}Ti_{44.7}Hf_{10}Pd_5$ (at.%). Their transformation temperatures, microstructure and shape memory properties were revealed and compared with conventional shape memory alloys. It was revealed that their transformation temperatures increases but transformation strain decreases with the increment of Hf content.

Additionally, superelastic responses of $Ni_{45.3}Ti_{29.7}Hf_{20}Pd_5$ and $Ni_{45.3}Ti_{39.7}Hf_{10}Pd_5$ alloys were investigated. Transformation temperatures of polycrystalline $Ni_{45.3}Ti_{29.7}Hf_{20}Pd_5$ are highly dependent on aging temperatures and they can be altered widely from room temperature to 250 ºC.

Finally, the damping capacity of the $Ni_{45.3}Ti_{39.7}Hf_{10}Pd_5$ polycrystal and [111]-oriented $Ni_{45.3}Ti_{29.7}Hf_{20}Pd_5$ single crystal were investigated. The damping capacities were found to be 16-25 $J.cm^{-3}$, and 10-23 $J.cm^{-3}$ for the $Ni_{45.3}Ti_{39.7}Hf_{10}Pd_5$ and [111]-oriented $Ni_{45.3}Ti_{29.7}Hf_{20}Pd_5$ alloys, respectively.

Keywords: NiTiHfPd, Smart Materials, High Temperature Shape Memory Alloys

Guher Pelin Toker

04/26/2018

CHARACTERIZATION OF THE SHAPE MEMORY BEHAVIOR OF

HIGH STRENGTH NiTiHfPd SHAPE MEMORY ALLOYS

By

Guher Pelin Toker

Haluk E. Karaca

Director of Thesis

Haluk E. Karaca

Director of Graduate Studies

04/26/2018

ACKNOWLEDGEMENTS

TABLE OF CONTENTS

LIST OF FIGURES

VIII

LIST OF TABLES

1. Chapter 1: Introduction

1.1 Motivation and Objectives

Throughout the centuries, metals, mainly steel and aluminum, have been used as structural materials in many applications. However, advanced technology and applications required high-performing materials. Thus, material scientists have investigated a new group of materials that would qualify as lightweight, multifunctional or multicomponent [1-3].

Smart materials are the branch of active or multifunctional materials which can possess more than one property with the aid of external signals such as temperature, stress, magnetic, electric field [2]. Shape memory alloys, magnetic shape memory alloys, piezoelectric ceramic and polymers are examples of such active materials [1].

Shape memory alloys have the unique ability to recover from large deformation by the removal of stress or heating. This phenomenon can be explained by the diffusionless solid to solid phase transformation, namely martensitic transformation. If martensitic transformation is reversible, it is called thermoelastic martensitic transformation [4]. During this thermoelastic martensitic transformation, material transforms from high-temperature parent phase (B2) to low-temperature martensite phase (B19') [5]. In other words, shape memory alloys can convert thermal energy to mechanical energy; thus, they can be utilized in numerous engineering applications in biomedical, aerospace, automobile and oil industries [1].

The most studied SMAs systems are Cu, Fe, and NiTi-based alloys. However; NiTi-based alloys are the workhorse of the SMAs because of their distinct superelasticity (SE) as well as their shape memory effect (SME) properties [6]. These properties are highly composition-dependent [7]. They also have excellent corrosion resistance and high damping capacity [6, 8]. While equiatomic NiTi alloys do not show good superelasticity, Ni-Rich NiTi alloys exhibit promising superelasticity because of the formation of precipitation. Besides this, transformation temperatures and strength of Ni-rich NiTi alloys can be controlled with thermal treatments thanks to the formation of precipitates [9].

Although NiTi alloys display promising properties, their low transformation temperatures (below 100 ^{o}C), poor strength and cycling stability are major challenges in many applications [4]. Low transformation temperatures and strength have limited the NiTi alloys to the applications that avoid high temperatures. For this reason, in order to alter the TTs and phase transformation mechanism, a third alloying element is added to NiTi binary system [10]. Hf, Zr, Pd, Pt, and Au are the most common alloying elements added to elevate the TTs. The alloys are named as High-Temperature shape memory alloys (HTSMAs). Hf and Zr are preferred among the other elements due to their relatively low cost [11]. NiTiHf and NiTiZr alloys had similar shape memory properties when they are compared to other high temperature shape memory alloys [12]. Ni-rich NiTiHf and NiTiZr alloys exhibit high mechanical strength and stable reversible transformation because of the precipitations [13]. Visible TTs chancing occurs above 10°C at-% in NiTiZr and NiTiPd/Pt alloys. Additions of Hf above 3% elevate the TTs, while up to 5-10 at-% hafnium results in 5 ^{o}C/at-% increases, and after that, it increases by 20°C/at-% [12]. Particularly, the addition of Hf up to 30% can elevate TTs up to 400 ^{o}C [14]. It is clear that Hf element is more effective on

2

the TTs of HTSMAs; however, brittleness of NiTiHf alloys is the main challenge in the applications; that is why quaternary elements such as Cu, Nb, Pd can be added to NiTiHf alloying system. Experiments revealed that addition of Pd to NiTiHf alloy has improved the ductility, shape memory properties and adjusted the TTs, as well [12]

The objectives and technical approaches to current study are to

- Study the effects of the addition of Pd into NiTiHf alloying system on their shape memory properties,

- Reveal the transformation temperatures, strain, hysteresis, microstructures, hardness and thermal cycling under compression responses of as-received (not applied post processing) NiTiHfPd alloys and they compare with aged samples,

- Study the influence of composition on the shape memory responses and TTs of NiTiHfPd alloys,

- Explore the effect of heat treatment time and temperature on the TTs and shape memory effect of NiTiHfPd alloys.

1.2   Brief history of Shape Memory Alloys

Shape Memory alloys was first discovered by A. Ölander as "smart alloys" in 1932 and Vernon described the term "shape memory" in 1941. Ölander found that the solid phase transformation in gold-cadmium (Au-Cd) alloys would deform when they cooled down, and would return to their prearranged shape when heated [15]. Later, Greninger and Mooradian noticed similar results in copper-zinc (Cu-Zn) and copper-tin (Cu-Sn) under thermal cycling [15, 16]. The thermoelastic martensitic transformation, which is the core phenomenon of shape memory effect, was governed by Kurdjumov and Khandros in 1949

and later by Chang and Read in 1951 [1, 15, 16]. In the early 1960s, William Buehler and his co-workers at the Naval Ordnance Laboratory (NOL) discovered the NiTi alloy and named it NiTiNOL [1]. Within two decades, SMAs, particularly NiTi became the preferred advanced material in many commercial applications thanks to their unique properties, above all, due to the fact that they exhibited good ductility, corrosion and wear resistance compared to most ordinary alloys [3, 5]. Later, HTSMAs such as TiPd, TiPt were developed at the beginning of the 1970s and they received a great deal of interest in the aerospace and oil industry. At the same time, other alloying elements such as Cu and Nb were added into NiTi alloys and research investigated their TTs and mechanical properties. Finally, another group of SMAs was discovered: besides the anticipated temperature and stress effects, these SMAs are sensitive to magnetic fields, and they can exhibit shape changes under magnetic fields. Magnetic SMAs also have great potential in actuator industries [1].

1.3   Background of Shape Memory Alloys

Shape memory alloys are a new class of metallic materials which have specific properties that make them more favorable compared to conventional materials. These alloys are unique because they can convert thermal energy into mechanical work and vice versa. After they mechanically deform at low temperature, these alloys can recover their original shape when having been heated to a certain temperature. They also demonstrate another mechanism that enables them to recover a large amount strain after they mechanically deform between their transformation temperatures [17].

SMAs have a capacity to solid-solid diffusionless thermoelastic phase transformation. SMAs go through two different phases with three different crystal

structures: twinned martensite (also referred to as self-accommodated martensite variants), detwinned martensite (also referred to as single variant martensite of reoriented martensite) and austenite phase. Austenite phase is known as a stable high-temperature phase, while martensite phase is known as an unstable, low-temperature phase [2, 15]. Temperature or external mechanic deformation results in the solid-solid transformation of SMAs. Based on this transformation, the main phenomenon of SMAs, namely Superelasticity (SE) and Shape Memory Effect (SME) will be detailed in the following sections.

1.4   Mechanism of martensitic transformations in SMAs

Phase transformation in SMAs can take place under either stress or changed temperatures. During the transformation, there are specific temperatures associated with the transformation. The martensite starts temperature (M_s) is the temperature where the martensite phase starts when the material is cooling down from austenite phase. Martensite finish (M_f) temperature is where the martensite-to-austenite transformation is completed upon cooling. Similarly, during heating, the martensite-to-austenite transformation starts at austenite start temperature (A_s) and then, at austenite finish (A_f) temperature, the material is completely in the austenite phase upon heating.

Figure 1.1. shows a typical DSC response of SMA. The calorimetric graph gives the transformation temperatures under zero stress condition. TTs can be determined by the tangential method. Upon cooling, material transforms to (partially or fully) detwinned martensite phase. During heating process, it will recover to the austenite phase.
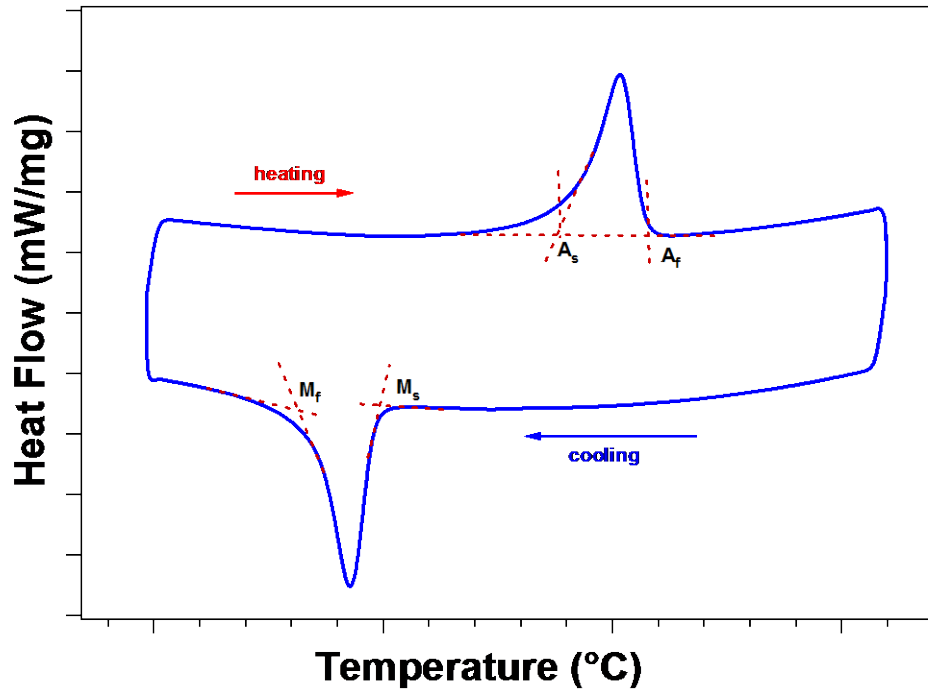
Figure 1-1 Typical DSC response

Figure 1.2 illustrates schematic of thermal cycling under stress. The constant stress is applied when the temperature is slightly above A_f, and it cools to below M_f, the transformation will result in the material to enter the martensite phase. When the material is heated above the A_f, complete shape recovery can be obtained. However, if the applied stress is enough for the plastic deformation, full shape recovery cannot be observed. TTs, total and irrecoverable strain, also temperature hysteresis can be obtained from the thermal cycling response and critical points were shown in Figure 1.2. It should be noted that since TTs are highly stress dependent, TTs can elevate with increasing stress level.

6
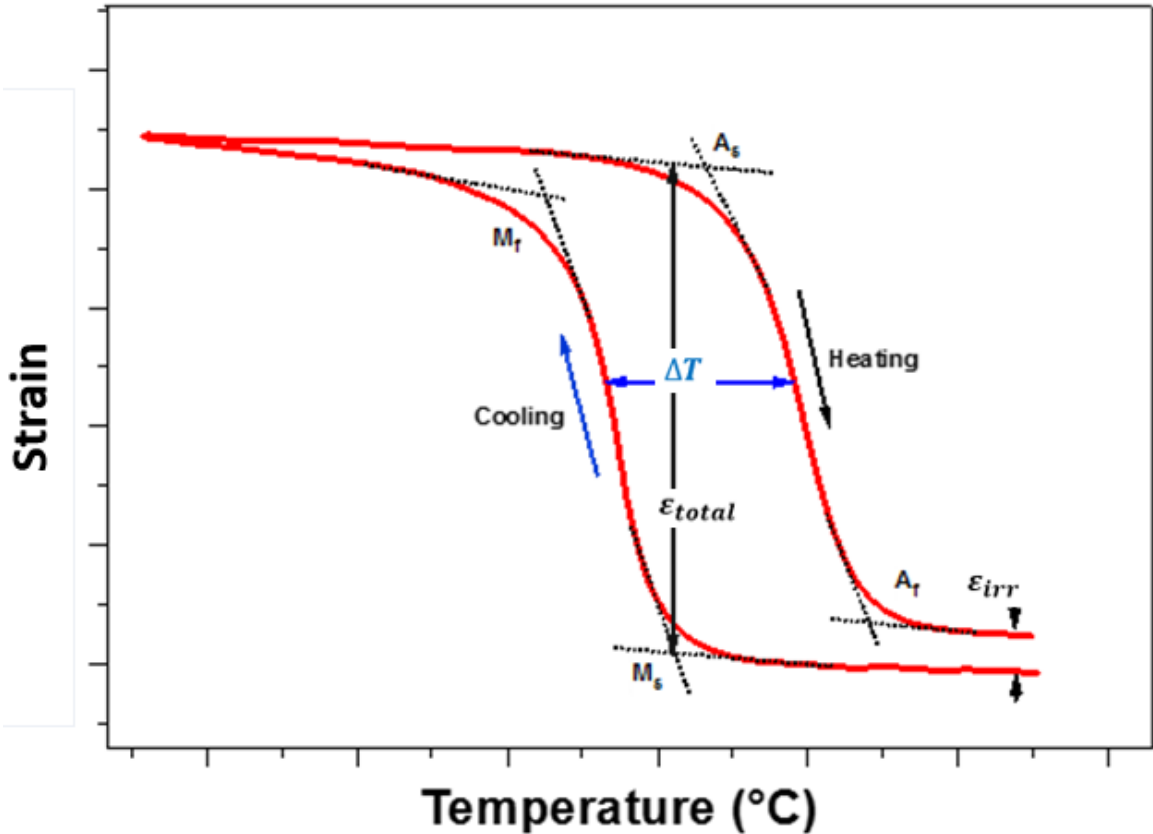
Figure 1-2. Schematic of thermal cycling under stress

1.4.1 Shape memory effect (SME)

Figure 1.3 (a) presents a schematic shape memory effect of SMAs. When the material is loaded at Mf temperature, twinned martensite transforms to detwinned martensite, and it is a macroscopic shape chance. When the load is released new configuration is retained at this temperature, full recovery cannot be observed. Subsequently, if material heated above A_f temperature, it could recover the retain strain while it transforms from detwinned martensite to austenite phase (Figure1.3b). This phenomenon is called shape memory effect (SME).
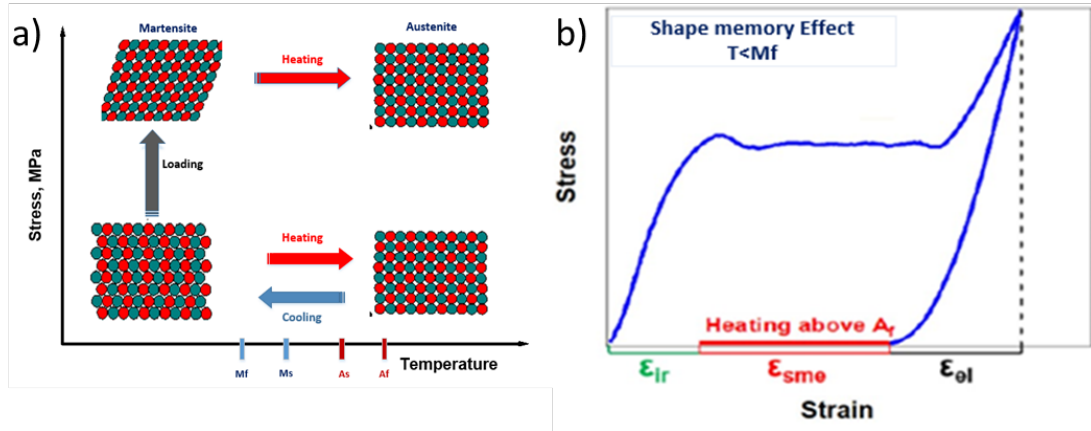
Figure 1-3 Schematic of shape memory effect behavior of SMAs

1.4.2 Superelasticity (SE)

Figure 1.4 shows a typical superelastic behavior in SMAs which takes places during the loading and unloading. When the material is in austenite phase (temperature is slightly above A_f), the inital linear part represents the elastic deformation of the austenite phase. Continued stress leads to phase transformation and plateau region is observed during the transformation from austenite to the martensite phase. When the stress is removed, reverse transformation martensite to austenite takes places. If there is no plastic deformation, fully reversible shape recovery can be observed. Young moduli and critical stress of austenite and martensite, superelastic strain and irrecoverable strain, mechanical hysteresis can be obtained from superelastic curves.

Superelastic behavior can be observed up to a certain temperature. If the temperature above M_d (martensite desist temperature), SMAs deform as conventional materials [18].

8
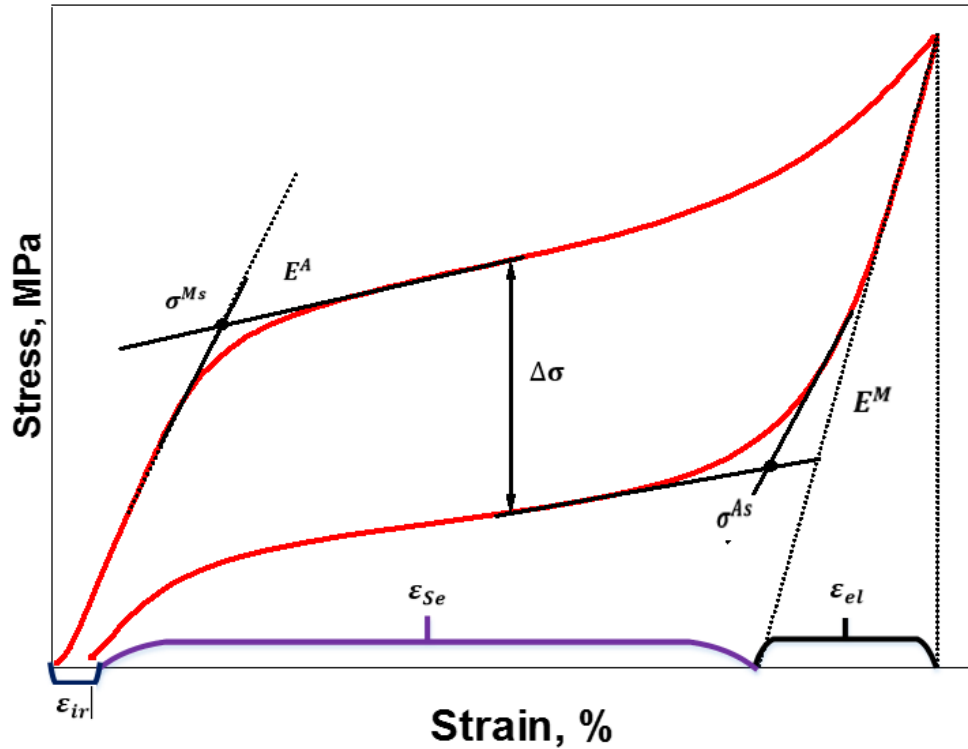
Figure 1-4 Typical SMA superelastic cycle

1.5 NiTi and NiTi-Based Shape Memory Alloys

1.5.1 Binary NiTi

NiTi (nitinol) alloys are the most studied and used shape memory alloys among the Cu and Fe- based SMAs because of their excellent mechanical properties, superelasticity and shape memory effect [6, 19]. NiTi alloys have the ability to recover strain of 8% or more depending on the test temperatures [20]. Martensitic transformation and their reversion make them a good candidate for many applications such as biomedical devices, implants, and deployable aerospace structures. SMAs display good wear, corrosion resistance, high specific electric resistance and high work density [7, 21, 22].

Near-equiatomic NiTi SMAs undergo three different phases which are the B2 austenite-A the monoclinic B'19 martensite (M) and the trigonal R-phase. Solution treated

9

near equiatomic NiTi displays a single stage transformation, namely, B2 to B'19 and B'19

to B2. When the materials expose certain condition such as cold working or aging R phase

could be emerged because of the precipitation formation [7, 22-24]. These three different

transformations display different properties, for instance, while B2-R transformation

exhibit very small strain (around 1%) and hysteresis, R-B19 and B2-B19 transformation

show highly large strain (up to 10%) [24].
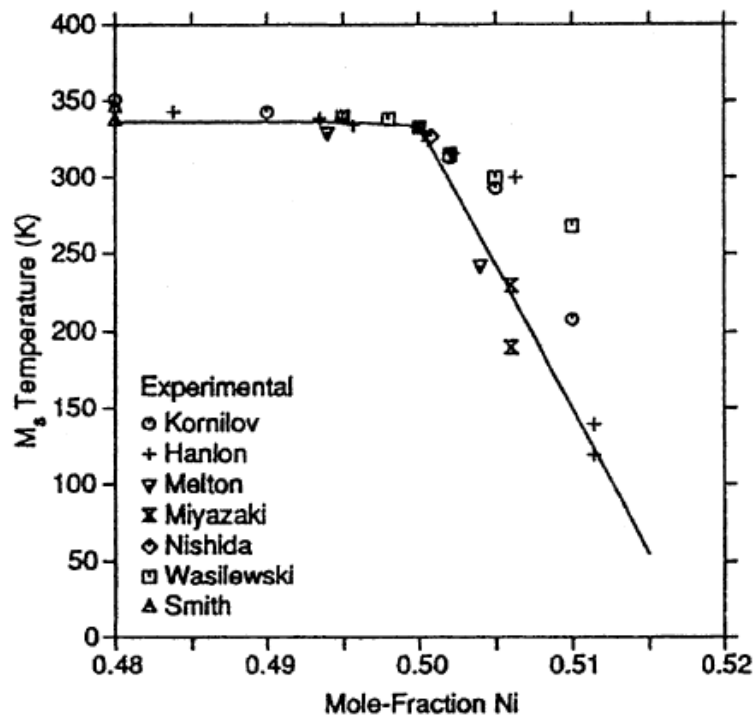
Figure 1-5 The chance of Ms temperatures as a function of Ni-content [25]

The Ni content in NiTi alloys has an essential role in altering the transformation

temperatures. Figure 1.5 shows that when the Ni-rich precipitates appear in the matrix, Ni

content decreases in the matrix, this results in increasing TTs [22]. Additionally, Ni-rich

precipitations effect the strength of NiTi matrix [4]. However, TTs cannot be altered of

near–equiatomic NiTi alloy because precipitation cannot be obtained by aging [25]. Also,

10

not only Ni content but also contamination such as oxygen and carbon affect the properties of NiTi alloys [7].

As shown in Figure 1.6 the deformation of shape memory alloys is highly temperature dependent because of the martensitic transformation. Below the A_f temperatures full recovery cannot be obtained and materials plastically deformed. If the material heated above the critical transformation temperatures, it will be deformed as conventional materials [26].
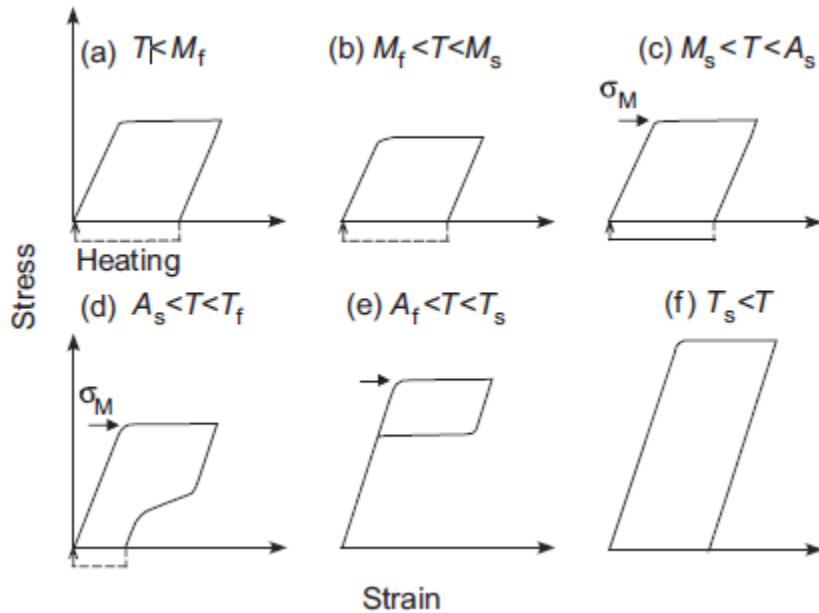
Figure 1-6 Schematic stress-strain curves of Ti-Ni alloy at different temperatures [26]

The composition is also one of the main parameters on the SMAs properties; highly Ni-rich NiTi alloys show high strength and toughness as compared the equiatomic NiTi alloys [27]. Shape memory behaviors of Ni-rich $Ni_{54}Ti_{46}$ alloys have been investigated by Karaca and et al. [27]. It was found that aged at 550 ^oC for 3hr Ni-rich NiTi alloys exhibited 3% superelastic response under high stress of 1500 MPa. Another ultra Ni-rich $Ni_{60}Ti_{40}$

alloys have been investigated by Kaya and et al. [28], and they obtained that 1.4% recoverable strain under 1000 MPa for 600 ^{0}C-3h aged alloys.

1.5.2   High-Temperature Shape Memory Alloys (HTSMAs)

The beginning of the development of SMAs has been used in the applications with operating temperature below 100 ^{o}C. However, developing the technology and increasing the needs in specific applications such as aircraft, oil and automobile industry require high transformation temperatures. These demanding push the scientists to new development in SMAs and new shape memory alloying system emerged as a High-Temperature Shape Memory Alloys (HTSMA) [1]. Thus, HTSMAs have been widely investigated not only their high transformation temperatures but also good cycling stability, creep and plastic deformation resistance. Furthermore, poor workability because of the secondary phases and relatively small transformation strain are their main challenges. However, those drawbacks could be overcome with thermal treatment, and alloying [12].

Alloying is one of the most powerful ways to improve the properties of NiTi alloys [29]. Addition of the third element expands the applications which need more specific properties of NiTi alloys. Alloying influences the TTs, strength, ductility, and shape memory characteristics. For example;

- Fe, Cr, Co, Al can decrease the TTs,

- Hf, Zr, Pd, Pt, Au increase the TTs,

- Cu and Nb can alter the hysteresis, [30]

Addition of Cu to NiTi alloys reduces the pseudoelastic hysteresis and also decreases the transformation strain. NiTiCu alloys are an ideal material for actuator due to

12

the small hysteresis. In contrast to the actuators, some applications need large hysteresis. Addition of Nb to NiTi alloys provides the wide thermal hysteresis. Moreover, also, NiTiNb alloys can be deformed at low temperatures. This alloys with around 3% Nb contents have shown good SME responses [1].

NiTiPd alloys have considerable attention between the HTSMA. Initially, Pd element had been added only for elevating TTs, however; recently, researchers have focused on their work output and dimensional and thermal stability. TTs can be tailored by replacing Ni with Pd in the alloying system. Figure 1.7 shows the Pd concentration and TTs relation. It is clear that when the Pd content higher than 10% in the system, transformation temperature raised linearly.

Additionally, the thermal stability of NiTiPd alloys studied, and it was observed that these alloys display better thermal stability after 1000 cycling. While the TT of NiTiPd changed only 2 °C after 1000 cycling, 30 °C change were observed in NiTi alloys after 1000 cycling [12, 30]
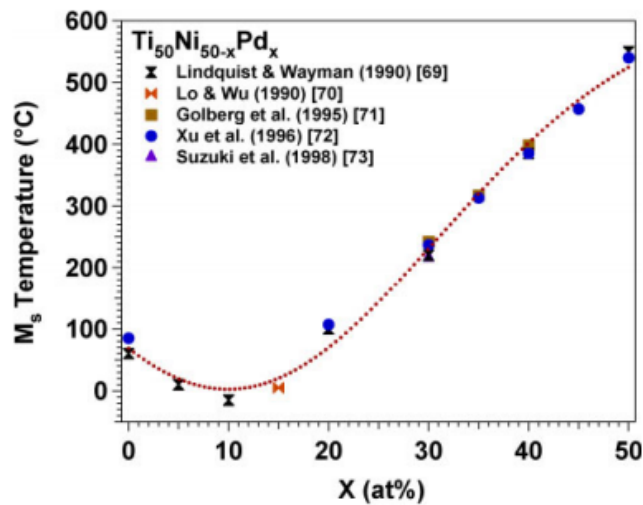
Figure 1-7 M_s temperature as a function of Pd content [12]

In particular, NiTiHf and NiTiZr are more investigated among the HTSMAs, because they are cheaper alternatives to Pd, Pt, and Au [13]. Although NiTiHf and NiTiZr display very similar shape memory response, Hf content is more efficient on the alloying system. If the Zr content is higher than 10%, transformation temperatures are raised at 18 °C/at %Zr. Moreover, also, when the Zr content is 20%, this alloy displays full recovery and it decreases with increasing Zr contents. However, up to 3%, Hf addition to NiTi binary alloys can elevate the transformation temperatures, and TTs start to increase after 5% Hf. Figure 1.8 shows the martensitic peak temperatures (M_p) as a function of Hf and Zr content in the ternary NiTiX alloying system. It is clear that in all the studies, the addition of Hf content above 10% cause the dramatic increases in transformation temperature [12, 30].
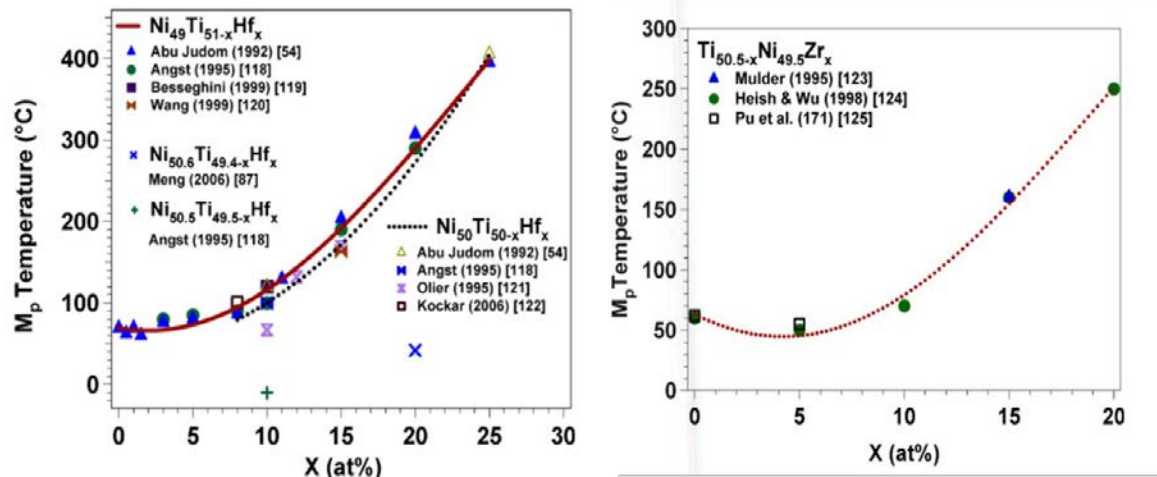
Figure 1-8 Martensitic peak temperatures as a function of a) Hf and b)Zr content [12

1.5.3 NiTiHf-X Alloys

NiTiHf alloys have considerable attention among the SMAs because they are relatively cheap compared to Pd andPt and TTs can reach up to 400 °C for Hf content up to 30 at% [14, 31]. However, particularly, Ni lean NiTiHf alloys have several drawbacks,

poor thermal stability, brittleness and low strength and these handicaps limited their actual applications [32]. Even though they are good candidates for high temperatures application, low ductility and strength are also significant challenges. Therefore, quaternary elements are added to NiTiHf alloys overcome their limitations.

Recently, Cu was investigated as one of the quaternary alloying elements into the NiTiHf alloys, NiTiHfCu alloying system was studied by Pasko et al. [33], and they observed that addition Cu was highly improved glass forming ability and superelasticity behavior. Another study was conducted by Liang et al. [34] they noted that NiTiHfCu alloys with three different compositions showed two-way shape memory behavior. They also showed exceptional thermal cycling stability.

Karaca et al. also investigated the addition of 5% Cu to NiTiHf alloys replacing Ni. They figured out that NiTiHf5Cu alloys can be a candidate for high-temperature application because their TTs can be elevated from $100^{o}C$ to $200^{o}C$ with the heat treatments. Furthermore, 0.8% two-way shape memory strain was obtained above the $80^{o}C$ [35].

Nb is also added to NiTiHf alloys to alter the properties of alloying systems. Kim et al [36] added to Nb to NiTiHf and investigated its cold workability. They observed that addition of Nb to NiTiHf alloys improved the cold workability and shape recovery; however, it caused to decrease TTs and plastic strain when Nb content decreased from 0 to 15% in NiTiHf. It was also revealed that increasing of the Nb contents result in increasing the recovery ratio, namely, while the Nb content was the recovery ratio was 60%, it was 90% when Nb content decreased to 15% in NiTiHf (Figure 1.9)
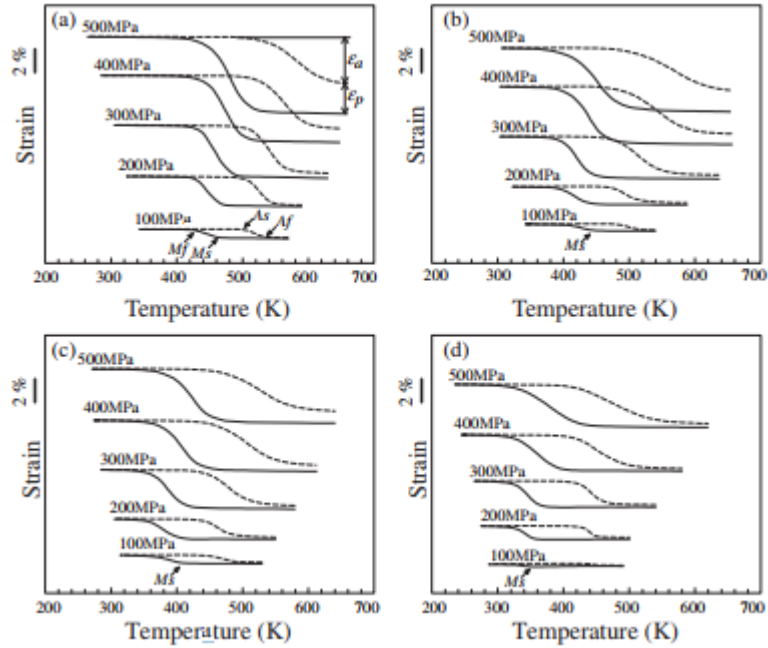
Figure 1-9 Thermal cycling response under constant stress (a) Ti– 49.5Ni–15Hf, (b) (Ti–49.5Ni–15Hf)–5Nb, (c) (Ti–49.5Ni–15Hf)–10Nb and (d) (Ti–49.5Ni–15Hf)–15Nb alloys [36].

Pd is another precious alloying element for NiTiHf alloys. The addition of Pd to NiTiHf alloy have played an important role on the TTs, shape memory properties as well as ductility of NiTiHf alloys. Addition of Pd can be resulted in increasing TTs as the expense of Ti or enhance the shape memory behavior as the expense of Ni in NiTiHfPd alloying system [29]. Recently, numerous studies have been carried out to reveal the effect of Pd in the NiTiHf alloys.

2. Chapter Two: Experimental Procedure

2.1 Introduction

This chapter describes the details of the technical equipment and experimental method used in the characterization of NiTiHfPd alloys. The material fabrication, preparation, microstructural analysis, calorimetric measurements and mechanical testing will be detailed throughout the chapter.

2.2 Material Fabrication and Preparation

EDM was used to cut compression samples ($8\times4\times4$ mm^3) and small pieces for DSC, hardness and microstructural analysis for each alloy. Figure 2.1 shows the employed KNUTH smart EDM.

Figure 2-1 KNUTH smart EDM

2.3 Heat Treatments

Lindberg/Blue M BF514541 Box furnace is used for heat treatments which is shown Figure 2.2. The furnace can reach to maximum temperature of 1200 °C. The samples were aged at a various temperature between 300°C to 800°C for 3 hrs followed by immediate water quenching at room temperature.

Figure 2-2 Lindberg/Blue M Box furnace (BF514841)

2.4 Calorimetry Measurements

Transformation temperatures (M_s, M_f, A_f and A_s) were measured using a Perkin Elmer Pyris 1 shown in Figure 2.3 differential scanning calorimeter (DSC). Typical temperature range is from -150 °C to 600 °C and the heating/cooling rate was 10 °C/min in a nitrogen atmosphere. Since the sample weight and preparation influence the measured TTs, a small amount of the materials (20-40 mg) should be used, and sample must be polished to obtain a good thermal contact. After polishing and weight measurement, sample kept in the aluminum pan before holding in DSC, and the other place was kept empty as a reference. The sample thermally cycled, and the difference of the supplied heat power was recorded. TTs are measured using a tangential method Figure 1.1

Figure 2-3 Perkin-Elmer DSC Pyris 1

2.5 Hardness Measurements

Microhardness measurements were obtained by Vicker microhardness 900-391D testing setup (Figure 2.4). 100 g-force was applied for 15 sec and then removed. Ten indentation measurements were recorded for each sample, the highest and the lowest measurements were discarded, and an average of 8 readings was reported
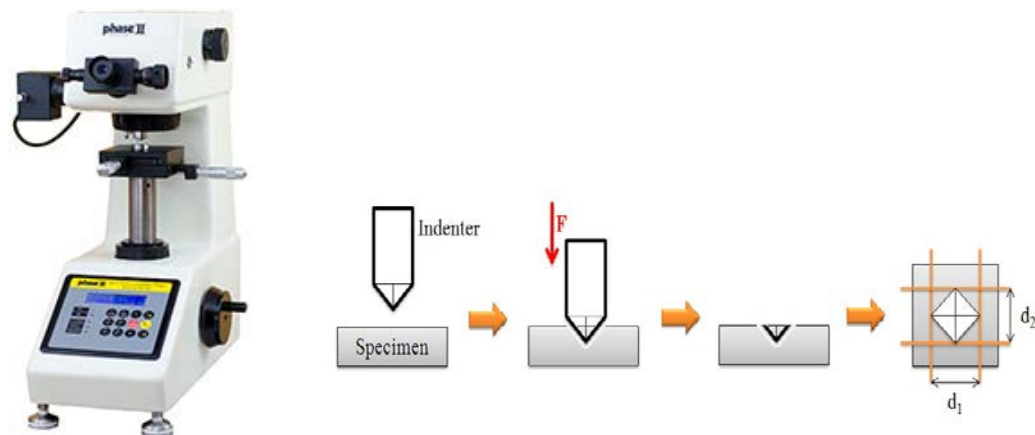
Figure 2-4 Metal-tester micro Vickers Hardness Tester 900-391D and Schematic of Vickers hardness measurement

2.6   Microstructural Analysis

For microstructural analysis, first samples were mounted using Epoxy resin and hardener and left for 8 hours for the solidification. For polishing, BUEHLER EcoMet/AutoMet 250 Grinder-Polisher was used that is shown in Figure 2.5. To achive the perfect surface, the grinding procedure has several steps including polishing with diamond suspensions of 9µm, 6µm, and 3µm. As for the final steps, alumina suspensions of 1µm and 0.5µm were used to obtain a smoother surface.

Figure 2-5 BUEHLER EcoMet/AutoMet250 Grinder-Polisher

Keyence VH_Z250 optical Microscopy was used to discover the microstructure of the samples (Figure 2.6). The polished samples were etched by H_2O (82.7%), HNO_3 (14.1%), HF (3.2%) (by volume) solution for various time period which is dependant on the composition of the alloy

Figure 2-6 Keyence VH_Z250R Optical Microscopy

2.7   Thermo-mechanical Tests

Thermos-mechanical compression experiments were conducted using the 100 KN MTS landmark servo-hydraulic test frame (Figure2.7). During the loading, a strain rate of 10^{-4} sec^{-1} was used while the unloading was performed under force control at a rate of 50 N/sec. The axial strain was measured by an MTS high-temperature extensometer which was attached to the top and bottom grips. Heating of the specimens occurred by means of mica band heaters retrofitted to the compression grips, at the rate of 5 ºC/min. Cooling was achieved through internal liquid nitrogen flow in the compression grips at 3 ºC/min rate. Omega CN8200 PID temperature controller was used for controlling the temperature, and three thermocouples were attached to the top and bottom grips of the MTS and to the

sample as well to provide real-time temperature recording during the experimentation
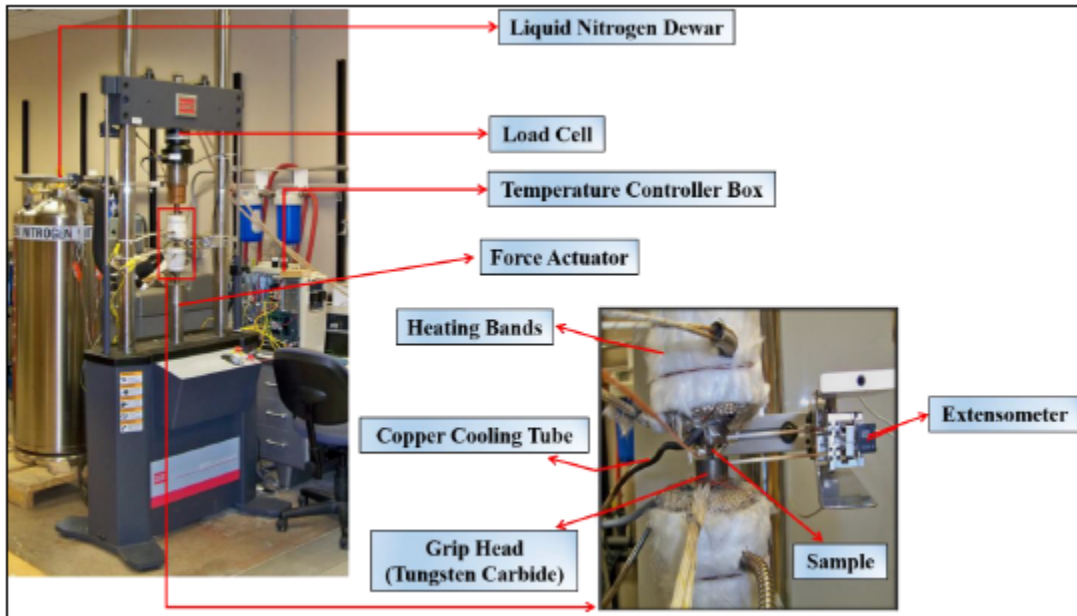
Figure 2-7 MTS Landmark servo-hydraulic test platform

3. Chapter Three: Effects of Composition on The Shape Memory Properties of Polycrystalline NiTiHfPd Alloys

3.1 Introduction

The aim of this chapter is to investigate the effects of chemical composition change (replacing with Hf) on the transformation temperatures (TTs), shape memory behavior and compressive stress responses of $Ni_{40.3}Ti_{34}Hf_{20}Pd_5$ $Ni_{40.3}Ti_{39.7}Hf_{15}Pd_5$ and $Ni_{40.3}Ti_{44.7}Hf_{10}Pd_5$ polycrystalline shape memory alloys. Additionally, microstructures of these alloys are revealed by optical and scanning electron microscopy. Distribution of secondary phases and composition also were discussed. For briefness, $Ni_{40.3}Ti_{34}Hf_{20}Pd_5$ $Ni_{40.3}Ti_{39.7}Hf_{15}Pd_5$ and $Ni_{40.3}Ti_{44.7}Hf_{10}Pd_5$ alloys will be called as NiTi20HfPd, NiTi15HfPd, and NiTi10HfPd throughout the section. Moreover, since any heat treatments have not been applied, these alloys will also be called as-received.

3.2 Phase Transformation alloys

Transformation temperatures provide the first idea and plan of the shape memory alloys. TTs are determined with DSC tests under zero stress, and they were measured from the curve which is shown in Figure 1.1. For each DSC cycle, higher temperatures represent the martensite to austenite phase; lower temperatures represent the austenite to martensite phase transformations.

Figure 3.1 shows the DSC graphs of as received NiTiHfPd alloys as a function of Hf contents. M_s temperatures of 127 °C, 48 °C, 19 °C and A_f temperatures of 162 °C, 107 °C and 98 °C were measured for NiTi20HfPd, NiTi15HfPd and NiTi10HfPd, respectively.
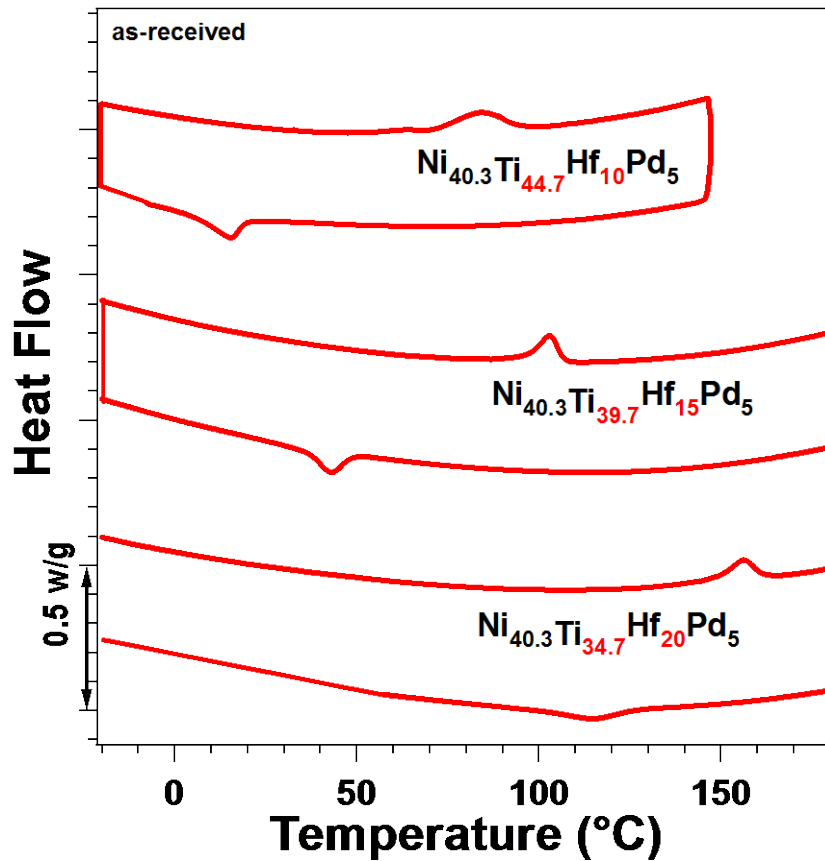
Figure 3-1 DSC responses of NiTi20HfPd, NiTi15HfPd, and NiTi10HfPd alloys

3.3   Microstructural characterization of NiTiHfPd alloys

Figure 3.2 shows the optical microscope images and SEM of the as-received NiTi15HfPd and NiTi10HfPd alloys. It is clear that secondary phases are homogeneously dispersed throughout the matrix. The chemical compositions of secondary phases and matrix were determined by EDS which is shown in Table 3.1. The secondary phases of all three alloys were found to be highly Ti-rich. While Ni and Ti contents of matrix of NiTi15HfPd andNiTi10HfPd are very close, the matrix of NiTi20HfPd is highly Ni-rich.

24
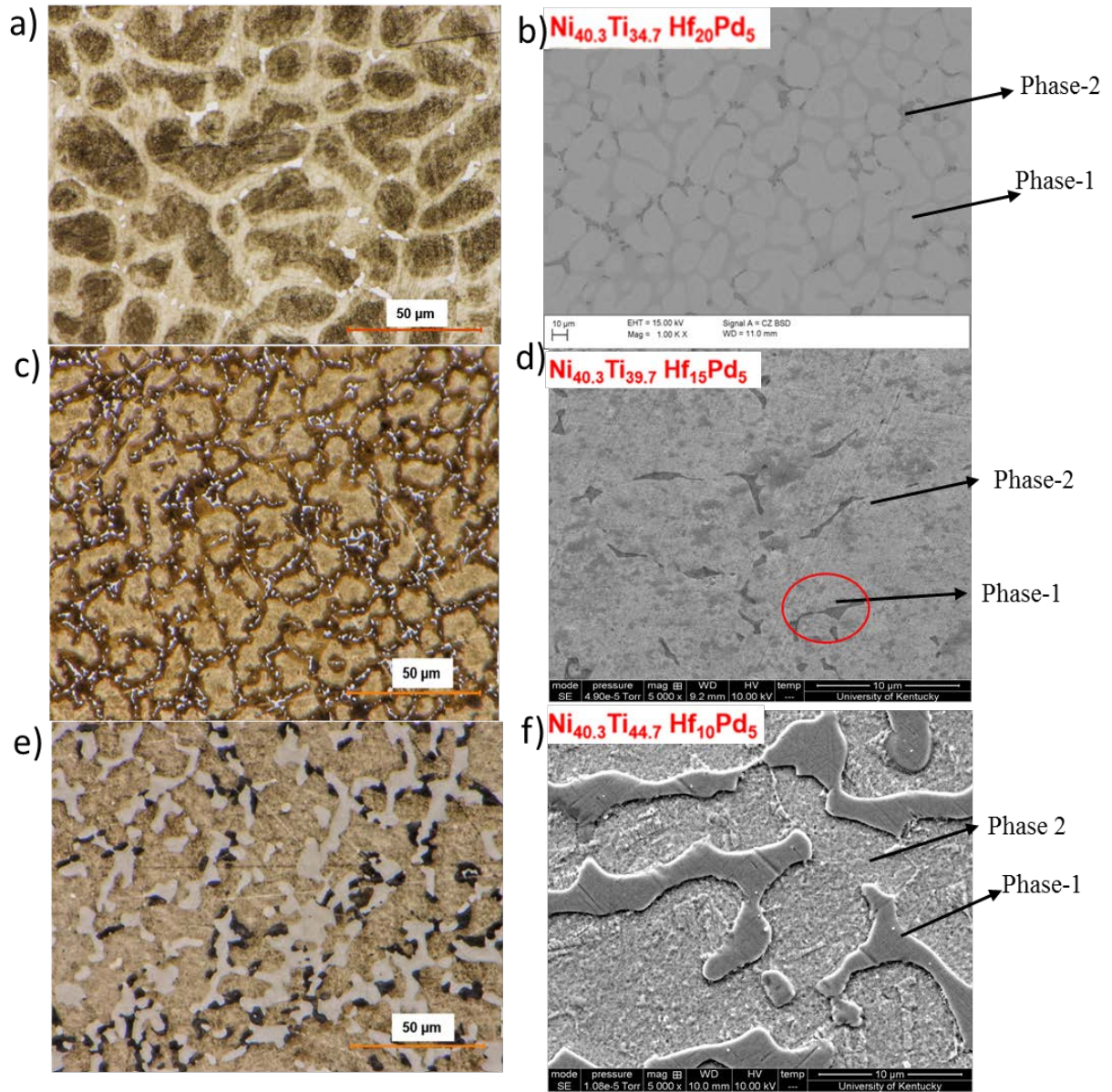
Figure 3-2 Optical microscopy and SEM images a-b) NiTi20HfPd, c-d) NiTi15HfPd and e-f) NiTi15HfPd

Table 3.1 EDS analysis of NiTi20HfPd, NiTi15HfPd and NiTi10HfPd

Element	Composition (at%)								
	NiTi20HfPd			NiTi15HfPd			NiTi10HfPd		
	Second Phase	Matrix	Overall	Second Phase	Matrix	Overall	Second Phase	Matrix	Overall
Titanium	49.97	27.84	36.14	50.8	40.9	40.4	52.3	41.3	47.3
Nickel	32.75	44.64	39.12	34.3	37.3	39.5	36.1	42.7	38.1
Hafnium	2.49	5.06	4.95	10.9	15.6	14.5	7.7	9.5	9.2
Palladium	14.79	22.46	19.79	4	6.2	5.6	3.9	6.5	5.4

3.4 Shape memory behavior

Figure 3.3 shows the thermal cycling under stress response of the as-received NiTiHfPd alloys. Each sample was thermally cycled between a temperature above A_f and a temperature below M_f under a constant stress. Once a thermal cycle was completed, the stress was increased, and then the samples were again thermally cycled. Transformation temperatures were measured by using tangential method; total, recoverable, irrecoverable strains were also obtained from thermal cycling curves, which is shown in Figure 2.2

Figure 3.3(a) shows the thermal cycling behavior of as-received NiTi20HfPd sample under constant stress. While very small recoverable strains were obtained, full recovery was not observed in this alloy. The recoverable strain of 0.20% and 0.22% and irrecoverable strain of 0.14% and 0.18% were measured at 700MPa and 1000 MPa respectively.

Figure 3.3(b) shows thermal cycling behavior of the as-received NiTi15HfPd alloy under compression. The Ms raised from 74 $^{\circ}$C to 88 $^{\circ}$C as the applied stress was increased from 300-1000 MPa. During the thermal cycling experiment, very small recoverable strain

of 0.43% was obtained at 700MPa. It showed full recovery up to 500MPa with 0.39% recoverable strain.

The thermal cycling responses of the as-received NiTi10HfPd alloy are given in Figure 3.3(c). The M_s increased from 47 °C to 90 °C alloys when the applied stress was raised from 300 to 1000MPa. Near perfect dimensional stability was observed up to 700 MPa with 0.23% irrecoverable strain. It also showed the recoverable strain of 1% and irrecoverable strain of 0.7% at 1000 MPa.
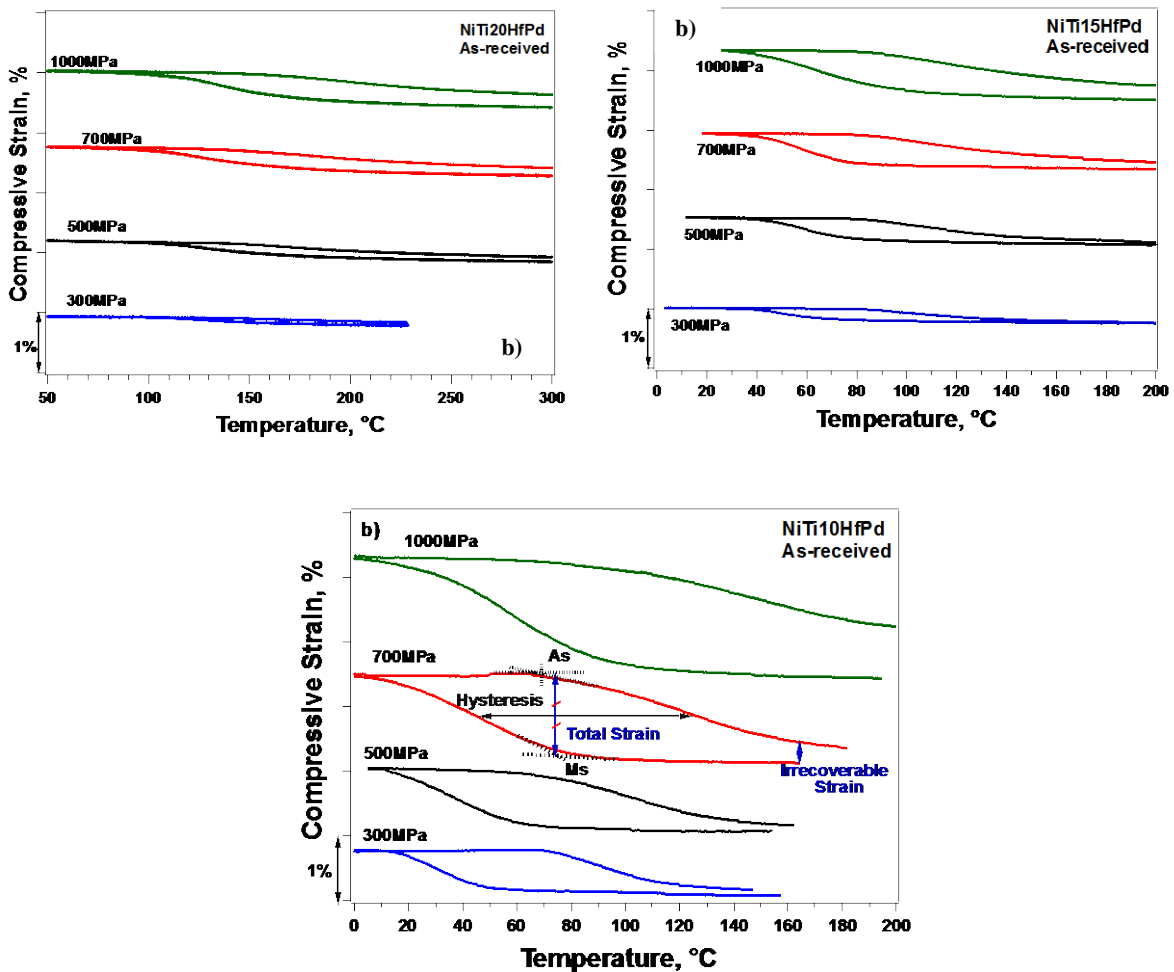
Figure 3-3 Thermal cycling under constants stress of as-received a) NiTi20HfPd, b) NiTi15HfPd and c) NiTi20HfPd alloys

27

3.5   Isothermal Stress-Strain Behavior of NiTi20HfPd and NiTi15HfPd

Figure 3.4 shows the stress-strain responses of as-received NiTiHfPd alloys. The NiTi20HfPd and NiTi15HfPd alloys exhibited fully recoverable superelasticity above the A_f, as the NiTi10HfPd showed full recovery even under A_f temperatures when it was loaded until 1100MPa.

Stress-strain responses of as received NiTi20HfPd sample illustrated in Figure 3.4 (a). All the tests were conducted above A_f and loaded up to 2% strain. While the full recovery was observed between 200 ^{o}C and 260 ^{o}C, plastic deformation is observed with 0.14% and 0.37% irrecoverable strain at 180 ^{o}C and 280 ^{o}C, respectively.

NiTi15HfPd as-received sample was loaded-unloaded above A_f temperature at 115 ^{o}C, 140 ^{o}C and 180 ^{o}C (Figure 3.4b). Full recovery was obtained in all three conditions while the sample was loaded up to 1200 MPa.

In contrast the NiTi20HfPd, NiTi15HfPd and NiTi10HfPd sample was tested below the A_f temperature and loaded up to 2% strain. It also showed full recovery except at 55 ^{o}C with 0.2% irrecoverable strain.
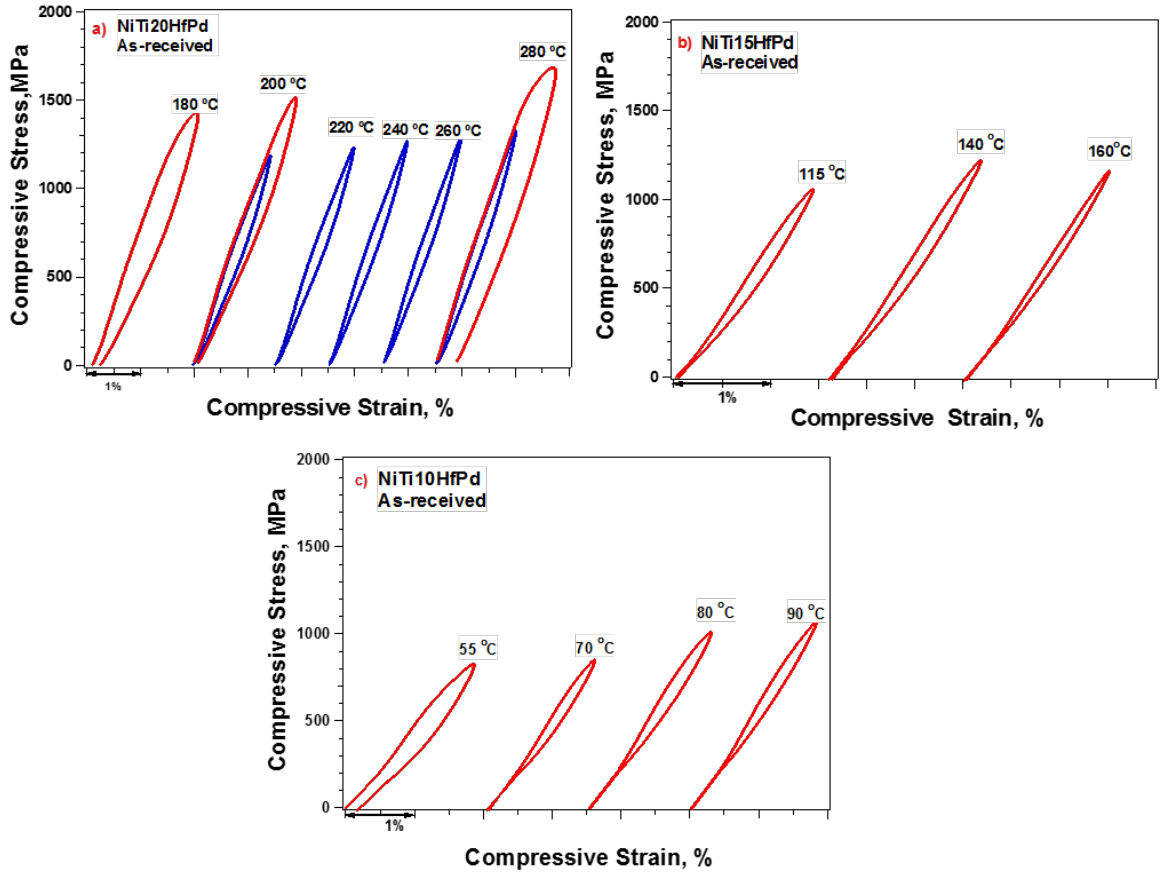
Figure 3-4 The compressive stress-strain response of as-received NiTiHfPd alloys as a function of temperature
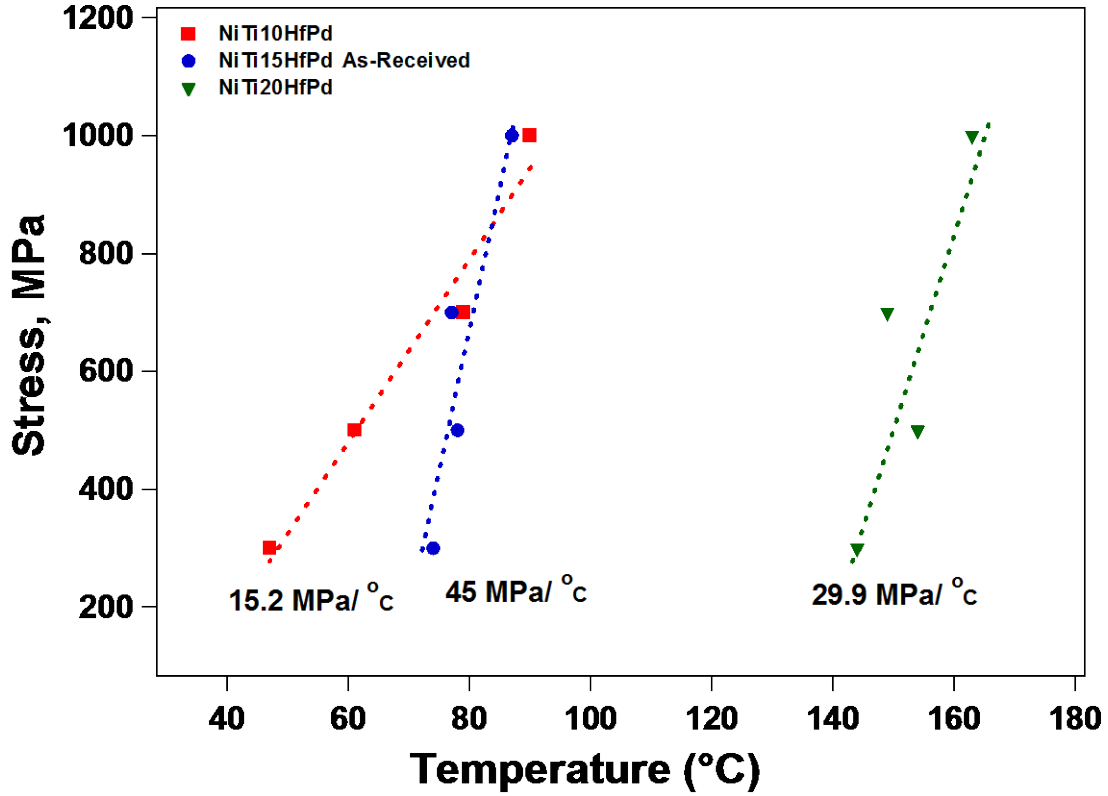
Figure 3-5 C-C relationship of as received NiTi15HfPd and NiTi10HfPd alloys (data were extracted from the heating-cooling curves)

The relationship between σ_{ms} and M_s can be determined by the Clausius-Clapeyron (C-C) equation [18] :

$$\frac{\Delta\sigma}{\Delta T} = -\frac{\Delta H}{\varepsilon_{tr}T_0}$$

$\Delta\sigma$ is the difference between critical stresses, ΔT is the temperature difference, T_0 is the equilibrium temperature and finally ε_{tr} is the transformation strain. The C-C slope was found to be 15.2MPa/ $^\circ$C, 45MPa/ $^\circ$C and 29.9MPa/ $^\circ$C for NiTi10HfPd, NiTiH15HfPd and NiTi20HfPd alloys. It is known that high C-C slopes are resulting in small and unstable recoverable strain and also lack of superelastic responses [32]. Thus, in the current study, while the C-C slopes of NiTiHfPd alloys are relatively higher than previous studies of

30

NiTiHfPd, recoverable strains are smaller. Previous studies have reported that C-C of as-extruded polycrystalline $Ni_{45.3}Ti_{29.7}Hf_{20}Pd_5$ alloys was 10.7MPa/ ^oC with the recoverable strain of 2.93% at 1000MPa [37]. C-C value of $Ni_{50.8}Ti_{49.2}$ alloys was reported as 11.5MPa/^oC with the recoverable strain of 3.26% under 300MPa constant stress [5]. It could be noted that NiTiHfPd alloys can be employed under high stress levels. The main reason of observing small strain in these alloys is the formation of secondary phases. Since they do not undergo phase transformation, they reduce the transformation strain. Thus, high volume fraction of secondary phases in the matrix results in less transformation strain. In Figure 3.2, Ti-rich secondary phases can clearly be observed, and these large secondary phases prevent the matrix to fully transform.
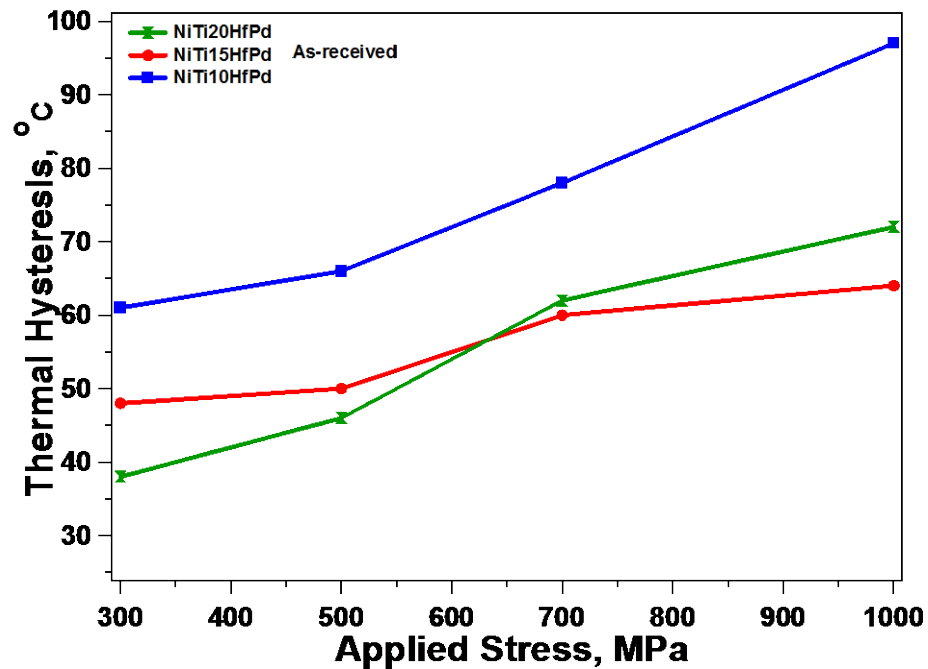
Figure 3-6 Thermal hysteresis of as-received NiTiHfPd alloys as a function of applied stress

The thermal hysteresis of NiTiHfPd alloys were measured from the heating-cooling curves and are shown in Figure 3.6. It is clear that thermal hysteresis increased with applied stress. Thermal hysteresis was measured as 38°C, 48 °C, and 61 °C at 300 MPa and 72 °C, 64 °C and 97 °C at 1000 MPa for as-received NiTi20HfPd, NiTi15HfPd and NiTi10HfPd, respectively. The thermal hysteresis of NiTi10Hf is determined to be larger than NiTi15HfPd. The thermal hysteresis is related to the compatibility of transforming phases and energy dissipation during the phase transformation [38]. Previous study also showed similar results where thermal hysteresis under 100 MPa were 17, 41, 72 °C for $Ni_{45.3}Ti_{29.7}Hf_{20}Pd_5$ $Ni_{45.3}Ti_{34.7}Hf_{15}Pd_5$, and $Ni_{45.3}Ti_{39.7}Hf_{10}Pd_5$ alloys, respectively [32]. We can conclude that, when Hf content increase in the alloying system, thermal hysteresis decreased.

3.6 Summary and conclusion

Effects of chemical composition on the transformation temperatures and shape memory properties were investigated in this chapter. The significant results have been summarized,

1. It was revealed that transformation temperatures increased as the Hf content increases into the alloying system. The M_s Temperatures were found to be 127 °C, 48 °C, and 19 °C for $Ni_{40.3}Ti_{34}Hf_{20}Pd_5$ $Ni_{40.3}Ti_{39.7}Hf_{15}Pd_5$ and $Ni_{40.3}Ti_{44.7}Hf_{10}Pd_5$, respectively.

2. Perfect recovery was obtained when the samples loaded with strain of 2% and stress level higher than 1GPa.

3. Relatively large secondary phases observed in the optical and SEM images and this secondary phase limited to obtain perfect recovery.

4. Clausius-Clapeyron relation were a strong function of Hf content, and the C-C slopes were found to be 15.2MPa/ ^{o}C, 45MPa/ ^{o}C and 29.9MPa/ ^{o}C for as-received NiTi10HfPd, NiTiH15HfPd, and NiTi20HfPd alloys, respectively.

5. Thermal hysteresis increased as a function of applied stress and Hf contents

4. Chapter Four: Effects of Aging on the Shape Memory Behavior of NiTiHfPd Alloys

4.1 Introduction

The purpose of this chapter is to investigate the influence of aging on the shape memory behavior of $Ni_{40.3}Ti_{34}Hf_{20}Pd_5$, $Ni_{40.3}Ti_{39.7}Hf_{15}Pd_5$, and $Ni_{40.3}Ti_{44.7}Hf_{10}Pd_5$ alloys. Transformation temperatures were determined after aging, the effects of aging temperature and time on the TTs were discussed. Hardness tests were conducted for all conditions and compared. Shape memory properties of $Ni_{40.3}Ti_{34}Hf_{20}Pd_5$, $Ni_{40.3}Ti_{39.7}Hf_{15}Pd_5$, and $Ni_{40.3}Ti_{44.7}Hf_{10}Pd_5$ alloys were revealed, and stress-strain and strain temperature responses were explained. For the briefness $Ni_{40.3}Ti_{34}Hf_{20}Pd_5$, $Ni_{40.3}Ti_{39.7}Hf_{15}Pd_5$ and $Ni_{40.3}Ti_{44.7}Hf_{10}Pd_5$ alloys were called NiTi20HfPd, and NiTi15HfPd NiTi10HfPd throughout the section.

4.2 Effects of Aging on the Transformation Temperatures

In this section, TTs of aged NiTi20HfPd, NiTi15HfPd, and NiTi10HfPd alloys were given. All the samples aged from 300 ºC to 800 ºC for 3 hours and TTs were determined as a function of aging temperature. Additionally, to observe the effect of aging duration, NiTi10HfPd samples were aged from 30 min to 10 hours at 500 ºC. All the stress-free DSC tests were employed for three cycles to verify the stability of the TTs. From ss-received to 500 ºC-3hr aging results were given at the graphs, rest of the TTs were shown at the comparison graph.

Figure 4.1(a) shows TTs of the NiTi20HfPd as a function aging temperature. Initially, TTs decreased when they aged between 300 ºC to 400 ºC then started to increase up to 500 ºC, after that dramatically TTs decreased again. When the aging temperature was

650 ºC, TTs started to increase again. The maximum and minimum A_f was found to be 265 ºC and 108 ºC at aged 800 and 350 ºC, respectively.
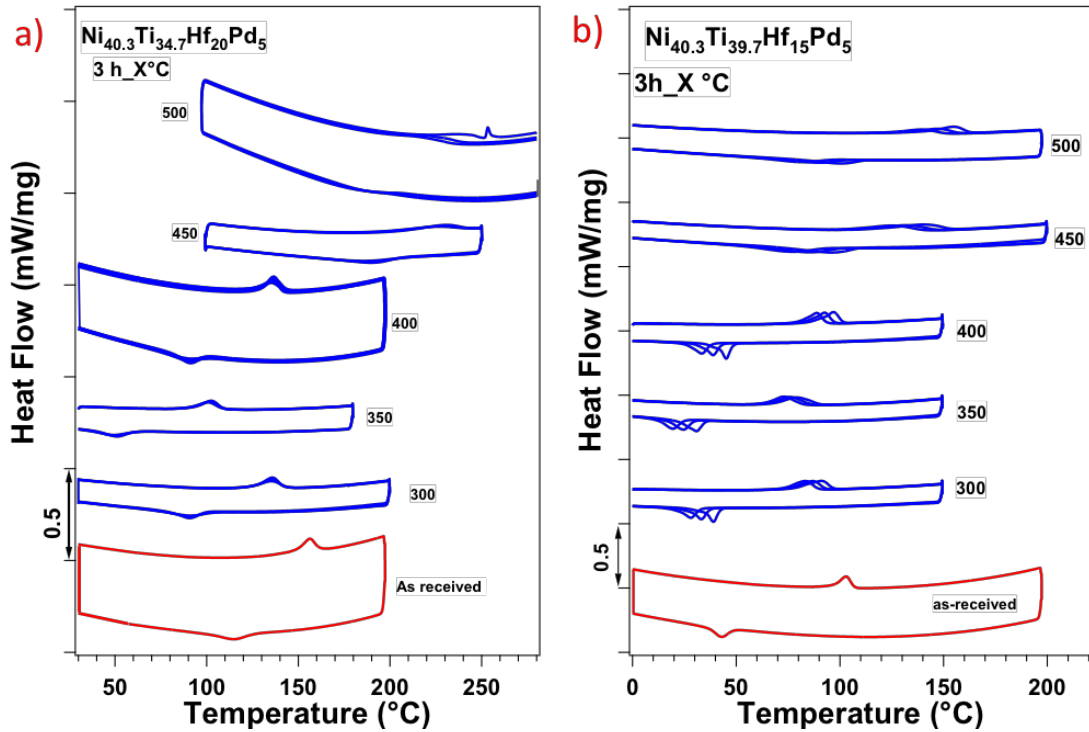
Figure 4-1 DSC responses of as-received and aged samples a) NiTi20HfPd and b) NiTi15HfPd

Figure 4.1 (b) shows DSC response of NiTi15HfPd alloy. This alloy showed very similar behavior with NiTi20HfPd. The maximum and minimum A_f temperatures were found to be 182ºC and 83 ºC aged at 800 ºC and 350 ºC for 3 hours, respectively.

Figure 4.2 (a) illustrates the TTs of NiTi10HfPd alloys aged for 3 hours. TTs slightly changed when they compared to NiTi20HfPd and NiTi15HfPd. Dramatic TTs changed was not observed in this alloy. Maximum and minimum A_f were measured from DSC curves, and they are 119 ºC and 66 ºC aged at 700 ºC and 350 ºC for 3 hours.
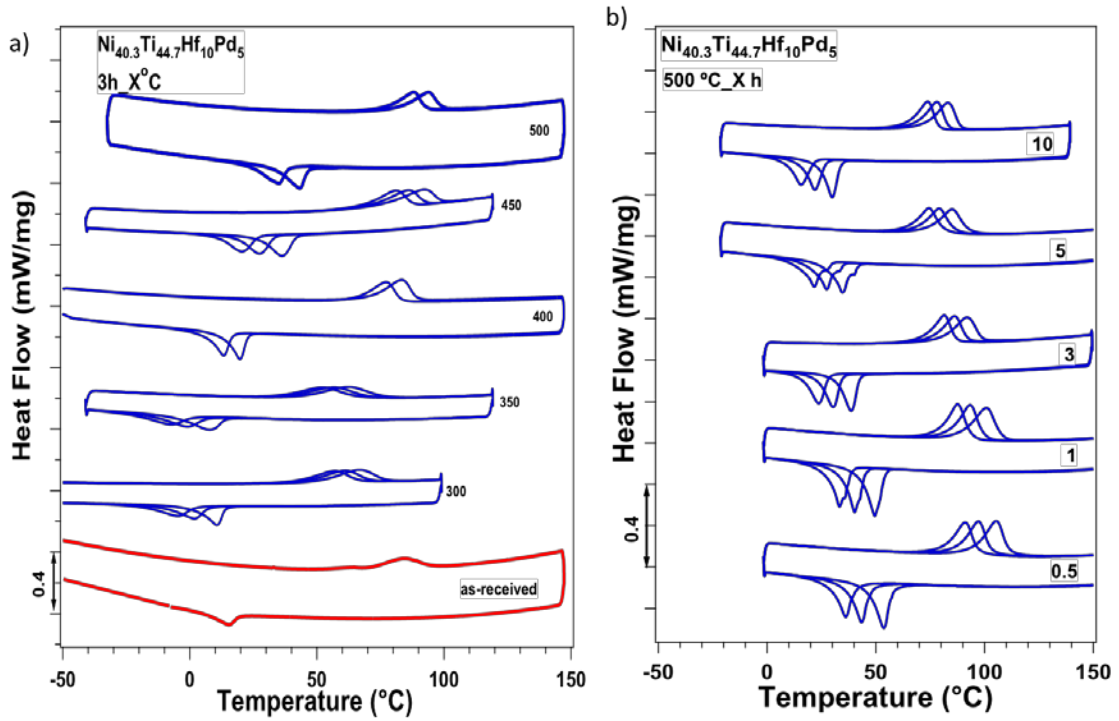
Figure 4-2 DSC responses of NiTi15HfPd as-received and aged samples as a function of a) temperature and b) duration time

TTs of NiTi10HfPd alloys as a function of aging time at 500 ^{o}C were shown in Figure 4.2 (b). In this study, aging temperature was kept constant as 500 ^{o}C while aging time was varied from 30 mins to 10 hours. It was observed that aging time does not affect on the TTs, but long aging time results a slightly decrease on the TTs. Under 500 C, the M_s temperature of aging time 30 mins and 10 hours were measured as 40 ^{o}C and 22 ^{o}C, respectively
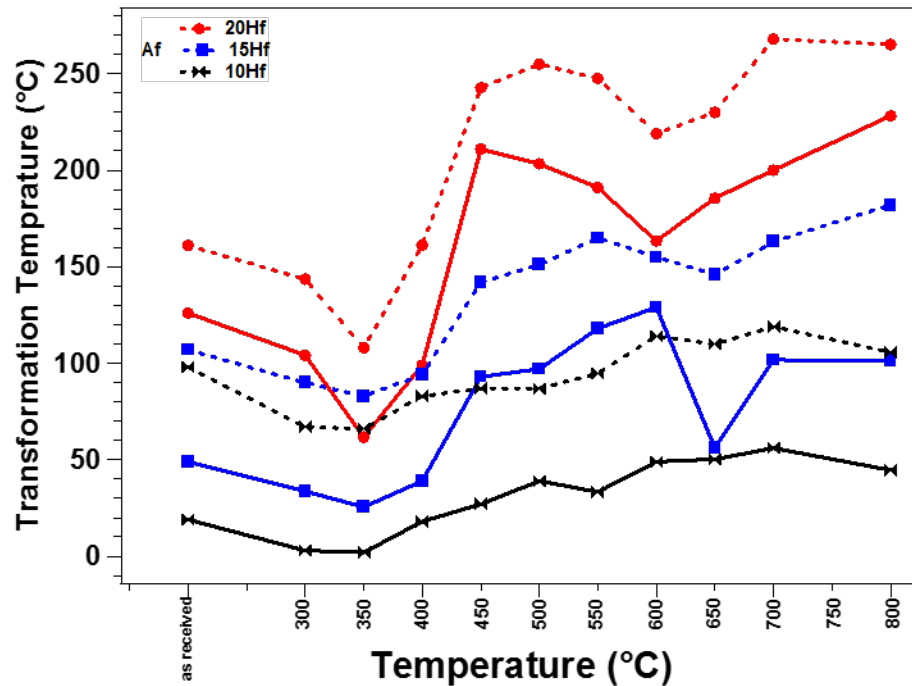
Figure 4-3 Comparison of TTs of NiTi20HfPd, NiTi15HfPd and NiTi10HfPd alloys as a function of various aging temperatures

Figure 4.3 illustrated the comparison of TTs of NiTiHfPd alloys aged at selected aging temperatures for 3 hours. The lowest TTs were observed aged at 350 $^{\circ}$C, the reason of this drop could be the formation of secondary phases. Since the secondary

It is clear that NiTi20HfPd showed the highest TTs among three alloys and its M_s temperature can be tailored between from 99 $^{\circ}$C to 228 $^{\circ}$C with the heat treatments. NiTi15HfPd exhibited similar TTs trend with NiTi20HfPd and sharp changing was observed in both alloys. However, TTs of NiTi10Pd were quite lower than other and slightly changed with the thermal treatments. The M_s Temperatures of NiTi10HfPd changed between 2 $^{\circ}$C to 50 $^{\circ}$C. It is known that higher than 3 at-% addition of Hf to NiTi results in increasing TTs. This increases around 5 $^{\circ}$C/at-% while the Hf content 5-10 %,

further addition of Hf dramatically elevates the TTs around 20 ^{o}C/at-% [12]. Thus, NiTi10HfPd alloy showed lower TTs than NiTi15FPd and NiTi20HfPd.

4.3   Hardness Measurements

Figure 4.4 compares the Vicker's hardness of NiTi20HfPd, NiTi15HfPd and NiTi10HfPd alloys as a function of aging temperature. All the experiments were carried out at room temperature, and thus all the samples were martensite. NiTi20HfPd and NiTi15HfPd alloys exhibit a similar trend. Also, Vicker's value of NiTi10HfPd alloys was lower than others. NiTi15HfPd and NiTi20Hf showed the lowest hardness value, while NiTi10HfPd has the highest value after 400 ^{o}C -3h aging.
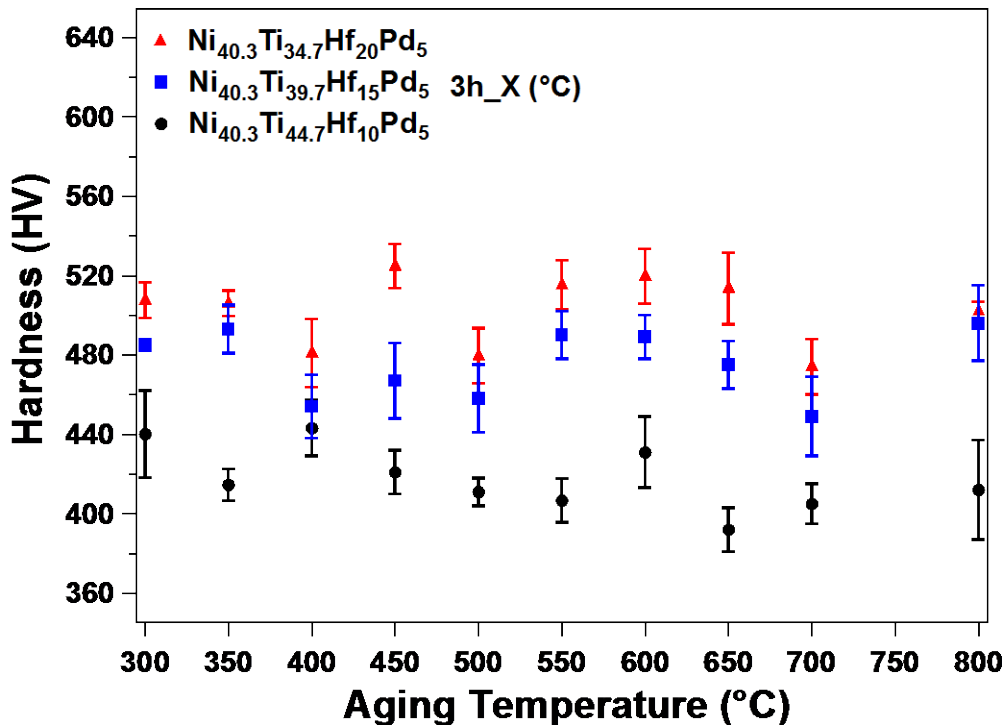
Figure 4-4 Vicker's hardness of NiTi20HfPd, NiTi15HfPd and NiTi10HfPd alloys as a function of aging temperature

4.4   Mechanical Responses of aged NiTiHfPd alloys

Figure 4.5 (a)-(b) illustrated that the shape memory response of the NiTiHfPd alloys aged at 350 °C for 3 h. NiTi15HfPd and NiTi10HfPd alloys showed almost perfect shape memory effect up to 500 MPa with irrecoverable strains of less than 0.2%. Irrecoverable strain increased when the stress level reached to 700 MPa with 0.3 and 0.6%, for NiTi15HfPd and NiTiHf10Pd respectively.
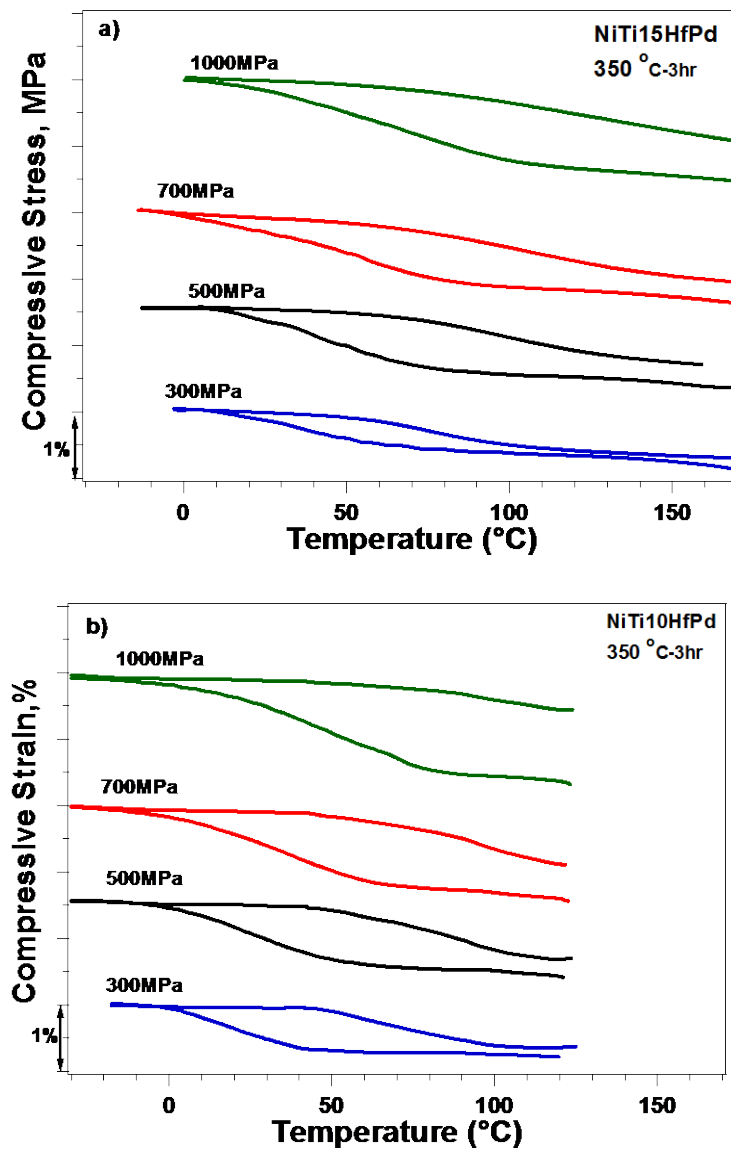
Figure 4-5 Thermal cycling of 350 °C -3h aged a) NiTi15HfPd, b) NiTi10HfPd alloys

Shape memory responses of 500 °C -3h aged NiTi15HfPd and NiTi10HfPd samples were depicted in Figure 4.6. While the applied stress increased from 400 to 1000 MPa, the M_s of NiTi15HfPd increased from 121 °C to 128 °C which is the highest M_s observed among all experiments. Additionally, NiTi15HfPd showed nearly perfect shape memory effect with 0.2% irrecoverable strain at 700 MPa. The Ms was 66 °C and 93 °C at 300MPa and 1000MPa, respectively. On the other hand, the irrecoverable strain of 0.25% was observed even at low stress of 300 MPa in NiTi10HfPd alloy
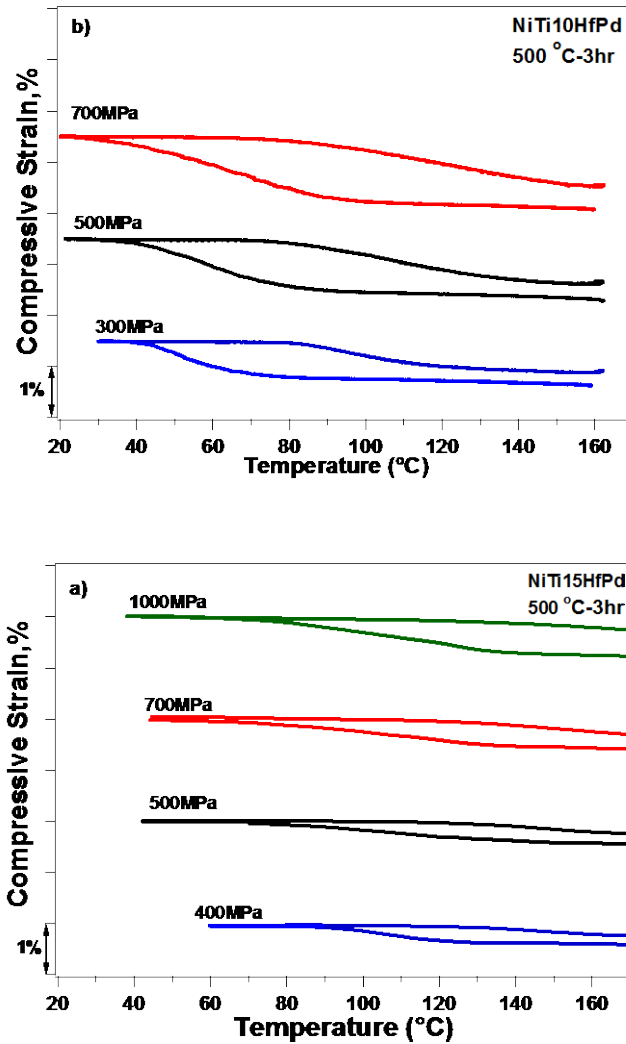
Figure 4-6 Thermal cycling of 500 °C -3h aged a) NiTi15HfPd, b) NiTi10HfPd alloys
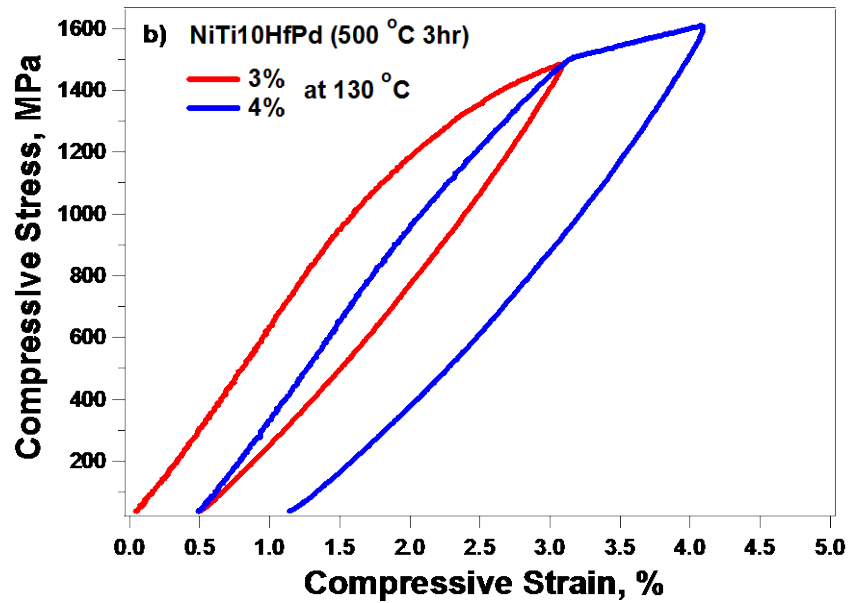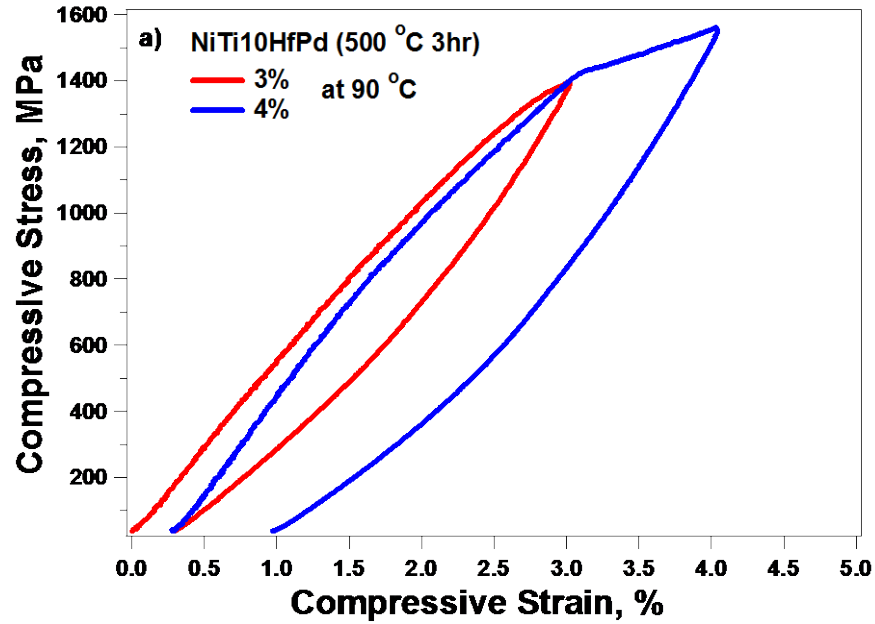
Figure 4-7 Compressive responses of 500 oC-3hr aged NiTi10Hf alloys at a) 90 °C, b) 130 °C

Figure 4.7 illustrates the compressive responses of 500 °C -3hr aged NiTi10HfPd alloys at 90 °C and 130 °C. To observe the superelastic behavior, sample was tested above the A_f temperature. When the sample was loaded up to 3% strain, irrecoverable strains were 0.3% and 0.5% at 90 °C and 130 °C, respectively upon unloading. With further loading

up to 4%, the irrecoverable strain of 0.69 % and 0.62 % were observed at 90 °C and 130 °C, respectively. It is clear from the graphs that high plastic deformation and strain hardening occurred at high-stress levels. Thereby, full recovery was not observed in NiTi10HfPd.
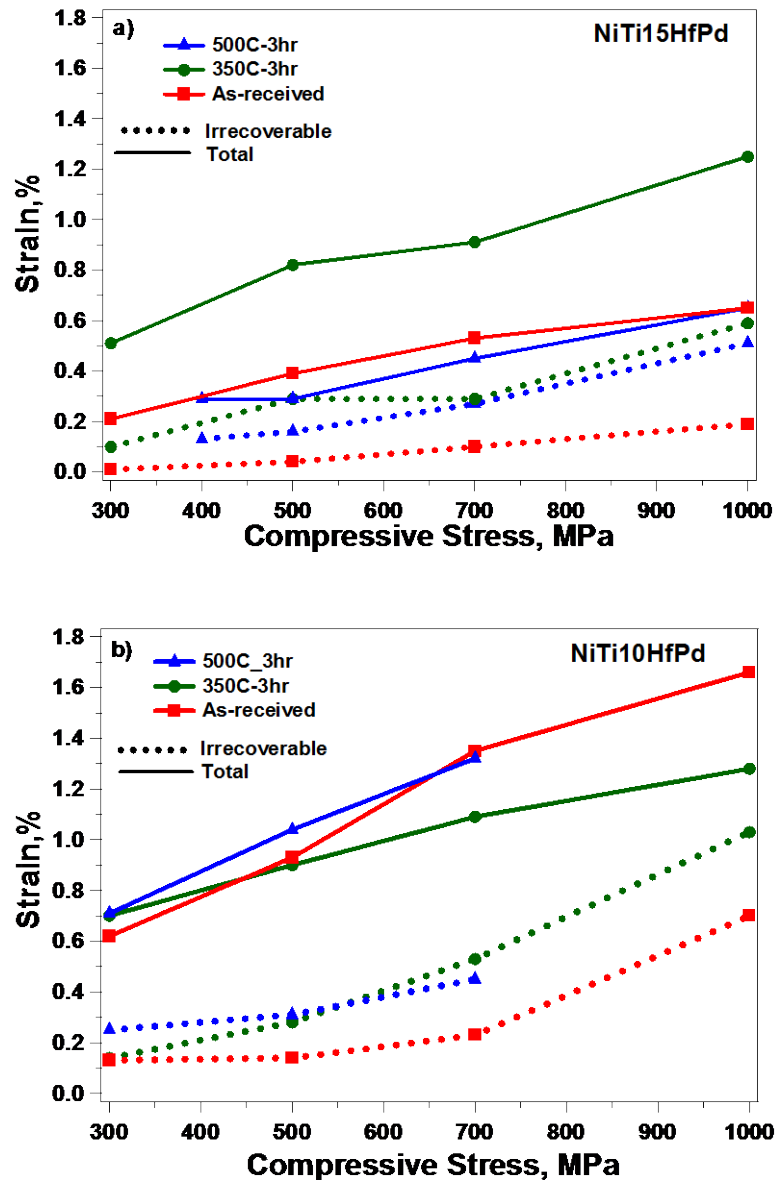
Figure 4-8 Total (solid line) and irrecoverable (dash line) strains as a function of the applied stress of as received and aged a) NiTi15HfPd, b) NiTi10HfPd alloys

Total and irrecoverable strains as a function of the applied stress of as received and aged NiTiHfPd alloys were given in Figure 4.8. While the as-received NiTi15HfPd sample showed very small recoverable strain of 0.4%, 350 °C -3hr aged sample showed highest transformation recoverable strain with 1% at 1000 MPa. Moreover, the total strain of as-received and 350 °C -3h aged and 500 °C 3h aged NiTi15HfPd were 0.53%, 0.91%, and 0.49% respectively, at 700 MPa, which is a good agreement with the hardness values of NiTi15HfPd. In contrast, NiTi10Hf as-received, 350 °C- 3hr and 500°C- 3hr aged samples showed very close strains and similar trend. Thus, heat treatments did not effect of NiTi10HfPd properties which are in good agreement DSC results.

4.5   Summary

In this chapter, mechanical properties and transformation temperatures were investigated as a function of aging temperatures and duration time. Following remarkable results can be explained;

1. Transformation temperatures of NiTiHfPd alloys can be tailored with the heat treatments. Moreover, these alloys can operate from room temperature to high temperatures (250 °C).

2. While the transformation temperatures of NiTi20HfPd and NiTi15HfPd alloys were affected by the aging temperatures, TTs of NiTi10HfPd were not significantly effected by heat treatments and its TTs slightly increased with aging temperatures. However, when the aging temperature kept constant at 500 °C, TTs of NiTi10HfPd decreased with aging time.

3. Hardness values of NiTi20HfPd and NiTi15HfPd are quite similar; however, NiTi10HfPd showed lower values.

4. 500 C- 3h aged NiTi10HfPd did not exhibited superelastic behavior with 0.3 and 0.5 % strain at 90 $^{\circ}$C and 130 $^{\circ}$C respectively when the sample loaded till 3% strain.

5. Fully shape memory recovery could not be achieved except NiTi15Hf aged at 350 $^{\circ}$C for 3 hours sample under 300 MPa. Very small recoverable strains were observed due to the presence of secondary phases.

5. Chapter Five: Shape Memory Behavior of $Ni_{45.3}Ti_{29.7}Hf_{20}Pd_5$ and $Ni_{45.3}Ti_{39.7}Hf_{10}Pd_5$ Alloy

5.1 Introduction

This chapter examines the shape memory properties of $Ni_{45.3}Ti_{39.7}Hf_{10}Pd_5$ and $Ni_{45.3}Ti_{29.7}Hf_{20}Pd_5$ alloys. Transformation temperatures and hardness values of as-received and aged $Ni_{45.3}Ti_{29.7}Hf_{20}Pd_5$ and $Ni_{45.3}Ti_{39.7}Hf_{10}Pd_5$ samples were determined. Temperature-dependent compressive responses of the as-received $Ni_{45.3}Ti_{29.7}Hf_{20}Pd_5$ and $Ni_{45.3}Ti_{39.7}Hf_{10}Pd_5$ samples have been revealed. Isothermal compression tests were conducted to observe the superelastic responses of the aged $Ni_{45.3}Ti_{39.7}Hf_{10}Pd_5$ alloy at selected temperatures (400 ºC, 500 ºC, and 600 ºC). Stress hysteresis and critical stress <u>were determined</u> as a function of test temperatures. Additionally, aged at 400 ºC- 3h $Ni_{45.3}Ti_{39.7}Hf_{10}Pd_5$ and [111] orientation $Ni_{45.3}Ti_{29.7}Hf_{20}Pd_5$ samples were tested at selected strain rates to reveal the damping capacity of those alloys. Since only a few studies conducted on the damping capacity and strain rate of $Ni_{45.3}Ti_{39.7}Hf_{10}Pd_5$ alloys, the systematic study provided the effect of the aging on the superelastic responses, critical stresses, stress hysteresis and dissipated energy of $Ni_{45.3}Ti_{39.7}Hf_{10}Pd_5$ and single crystal [111] $Ni_{45.3}Ti_{29.7}Hf_{20}Pd_5$ alloys.

5.2 Shape Memory Behavior of $Ni_{45.3}Ti_{29.7}Hf_{20}Pd_5$

Transformation temperatures of $Ni_{45.3}Ti_{29.7}Hf_{20}Pd_5$ were revealed with DSC as shown in Figure 5.1. Samples were aged for 3 hours from 300 to 500 ºC. A_f of the as-received sample was found to be 106 ºC, and TTs decreased to 400 ºC-3hr aging, and it was found to be 27 ºC for 400 ºC-3hr aging condition. After that, they sharply increased at

450 and 500 ºC-3hr. TTs increased to 203 ºC at 500 ºC-3hr aging. It was found that aging is an effective method to adjust TTs and they could be operated at a wide range of temperatures.
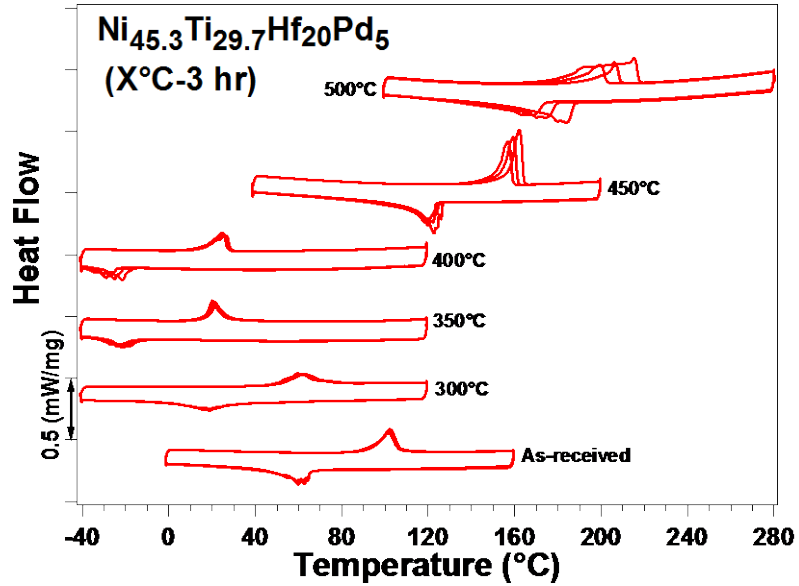
Figure 5-1 Transformation Temperatures of NiTi20HfPd as a function of aging temperatures
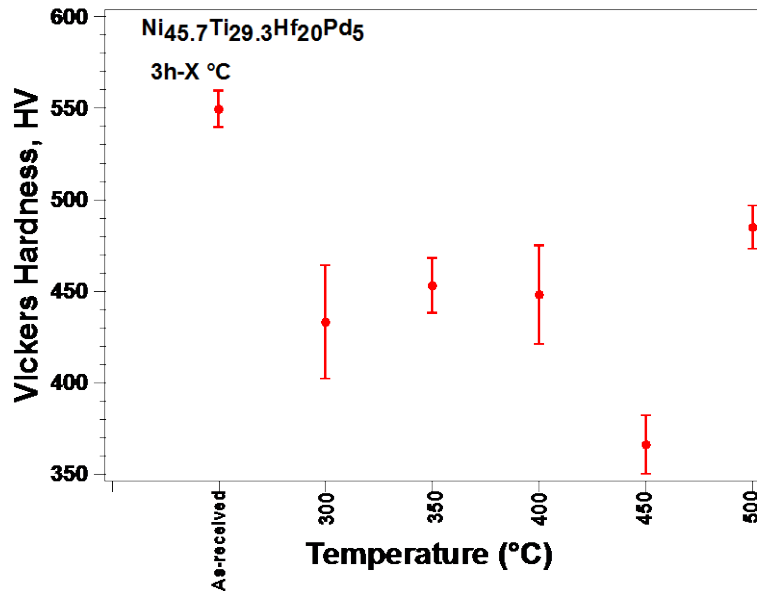
Figure 5-2 Vickers micro-hardness values of NiTi20HfPd alloys as a function of aging temperatures

46

Figure 5.2 shows the Vickers hardness of as–received and 3 hours aged NiTi20HfPd alloys. All the aged samples showed lower hardness values than the as-received condition. Vickers hardness values were very similar between at 300 °C to 400 °C aging conditions. However, hardness values sharply dropped after 450 °C-3hr aging.
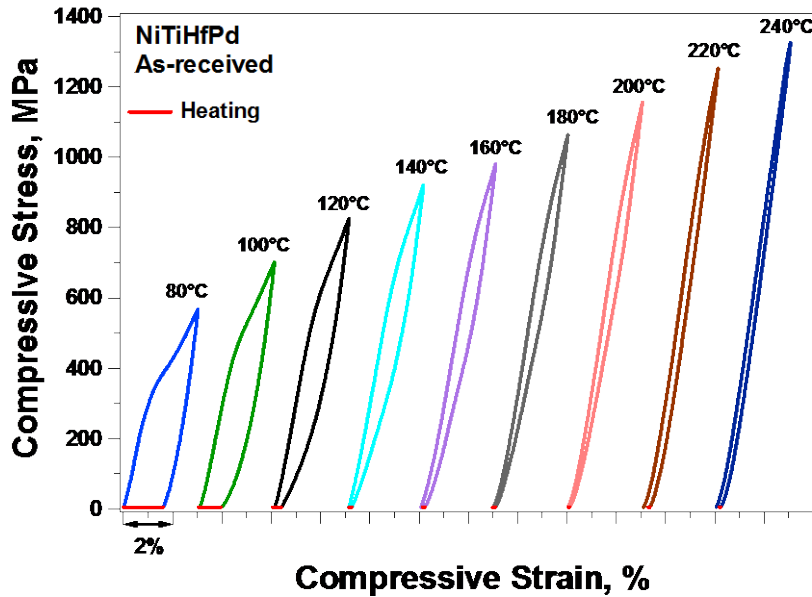
Figure 5-3 Temperature dependent compressive response of as-received
$Ni_{45.3}Ti_{29.7}Hf_{20}Pd_5$

Figure 5.3 shows temperature-dependent stress versus strain responses of as-received $Ni_{45.3}Ti_{29.7}Hf_{20}Pd_5$. As-received sample was simply loaded up to 3% strain and then unloaded. After each test, the sample was heated above the A_f temperature, and the irrecoverable strain was recovered after heating. The sample was not entirely austenite below 106 °C thus, below this temperature did not show full recovery after unloading. The same process was repeated as the test temperatures increased by 20 °C on each test. The sample showed almost full recovery at 120 °C which is above A_f temperatures.

5.3   Temperature Dependent Superelastic response of $Ni_{45.3}Ti_{39.7}Hf_{10}Pd$

As-received and aged samples of $Ni_{45.3}Ti_{39.7}Hf_{10}Pd_5$ alloy tested in this section. Samples were aged at selected temperatures, 400 ºC, 500 ºC and 600 ºC for 3 hours. Acar E. [4] has been determined transformation temperatures of the first batch of this alloy, and it was found to be -40 ºC. At each batch TTs and mechanical behaviors slightly are changed. For this reason, it was thought that TTs went to lower than -40 ºC based on the previous studied. Therefore, TTs of this alloy cannot be determined since DSC equipment which in the current lab can go to min -60 ºC. For this reason, TTs cannot be provide for the comparison.
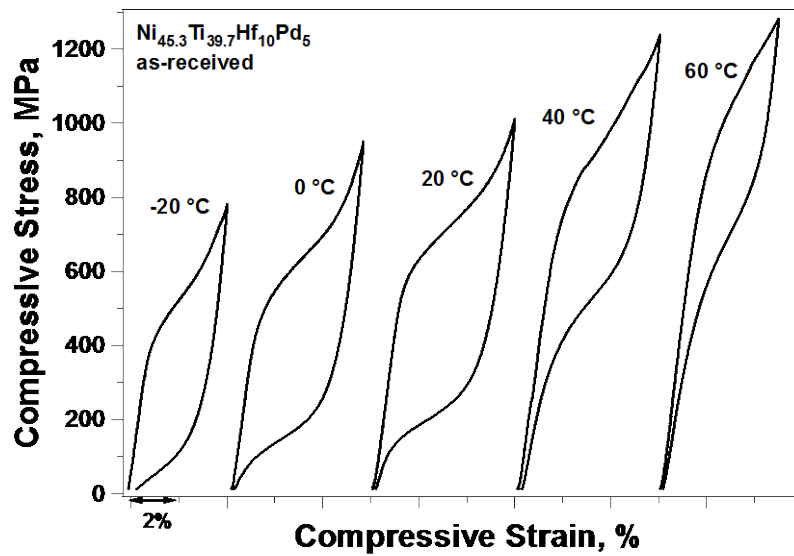
Figure 5-4 Temperature dependent stress-strain curves of as-received $Ni_{45.3}Ti_{39.7}Hf_{10}Pd_5$ alloy

Stress-strain curves response of as-received $Ni_{45.3}Ti_{39.7}Hf_{10}Pd_5$ alloy at various temperatures were given in Figure 5.4. Sample showed full recovery with strain of 6% between 0 ºC to 60 ºC.   The irrecoverable strain of 0.32% was determined at -20 ºC when

the sample loaded up to 5%. According to C-C relation the critical stress is temperatures dependent, and critical stresses linearly raised with the increasing of temperature.

Figure 5.5 illustrated the stress-strain responses of aged at 400 °C-3h, 500 °C-3h and 600 °C-3h Ni$_{45.3}$Ti$_{39.7}$Hf$_{10}$Pd$_5$ alloys in compression at selected test temperatures. Samples loaded up to strain values of 1 % then unloaded. After the completed cycle, the applied strain was incremented by 1%. This process was repeated until the applied strain of 5 % for each test temperatures. The last curves were displayed at graphs.
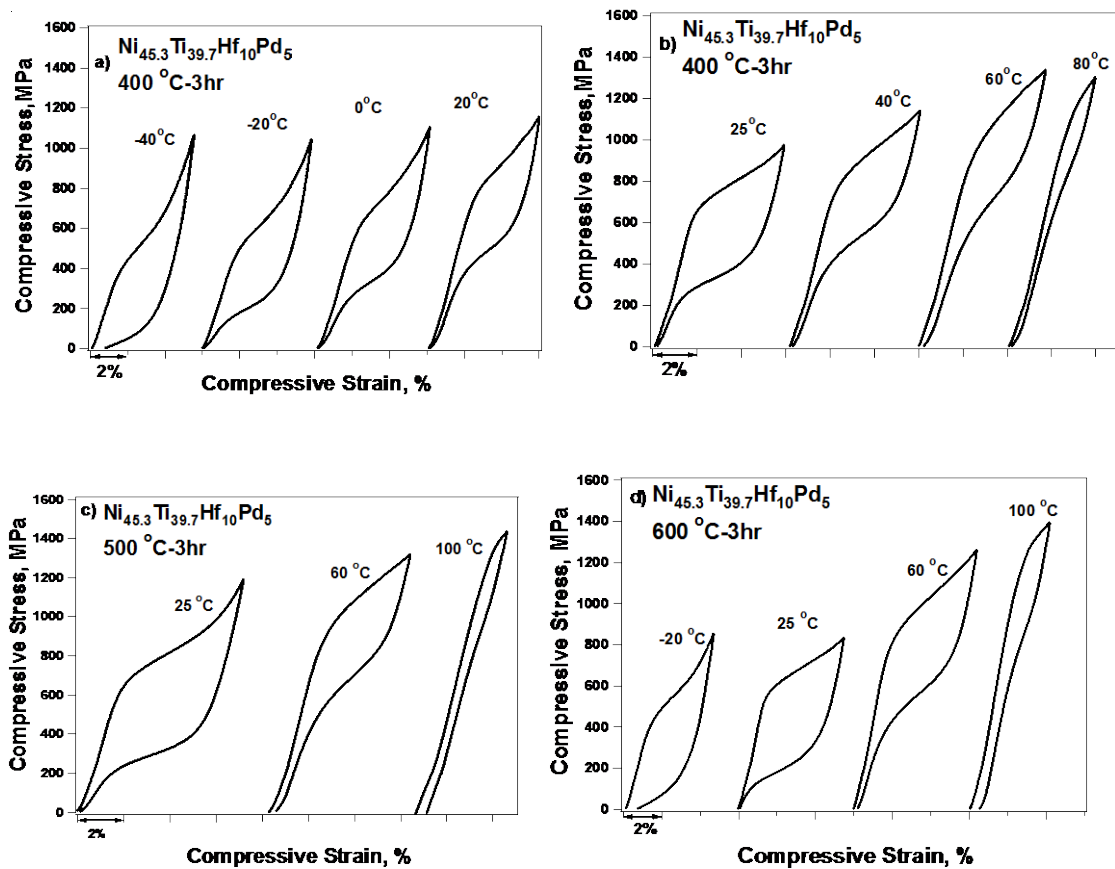
Figure 5-5 Temperature dependent stress-strain curves of Ni$_{45.3}$Ti$_{39.7}$Hf$_{10}$Pd$_5$ alloys at a) and b) 400 °C-3hr, c) 500 °C-3hr, d) 500 °C-3hr aged conditions

Stress-strain responses of aged at 400 °C-3h Ni$_{45.3}$Ti$_{39.7}$Hf$_{10}$Pd$_5$ alloy were given in Figure 5.5 (a-b). The temperature range was selected from -40 °C to 80 °C. Full recovery

was observed all the temperatures except -40 ºC in which irrecoverable strain of 0.71 % was observed. While the critical stress increased, plateau region was diminished as a function of temperatures.

Figure 5.5 (c) shows the compressive stress response of the sample aged at 500 ºC-3hr. Test temperature selected as a 25 ºC, 60 ºC and 100 ºC. The sample was loaded up to the strain of 5% and unloaded. Full recovery and high-stress hysteresis were obtained at 25 ºC. At the temperature of 60 ºC, almost full recovery was observed with the irrecoverable strain of 0.32%. However, stress hysteresis became narrow at this temperature. When the temperature increased to 100 ºC, work hardening was, and plastic deformation was observed with the irrecoverable strain of 0.77%.

Similarly, temperature dependent stress-strain responses of aged at 600 ºC-3hr sample were given in Figure 5.4 (d). The sample showed full recovery at 25 ºC and 60 ºC. However, at the temperature of -40 ºC irrecoverable strain of 0.64% was observed. This irrecoverable strain can be called a remained martensite, since the sample loaded at higher temperatures, it showed fully transformation. Sample was plastically deformed with an irrecoverable strain of 0.45% at 100 ºC, and work hardening was observed.
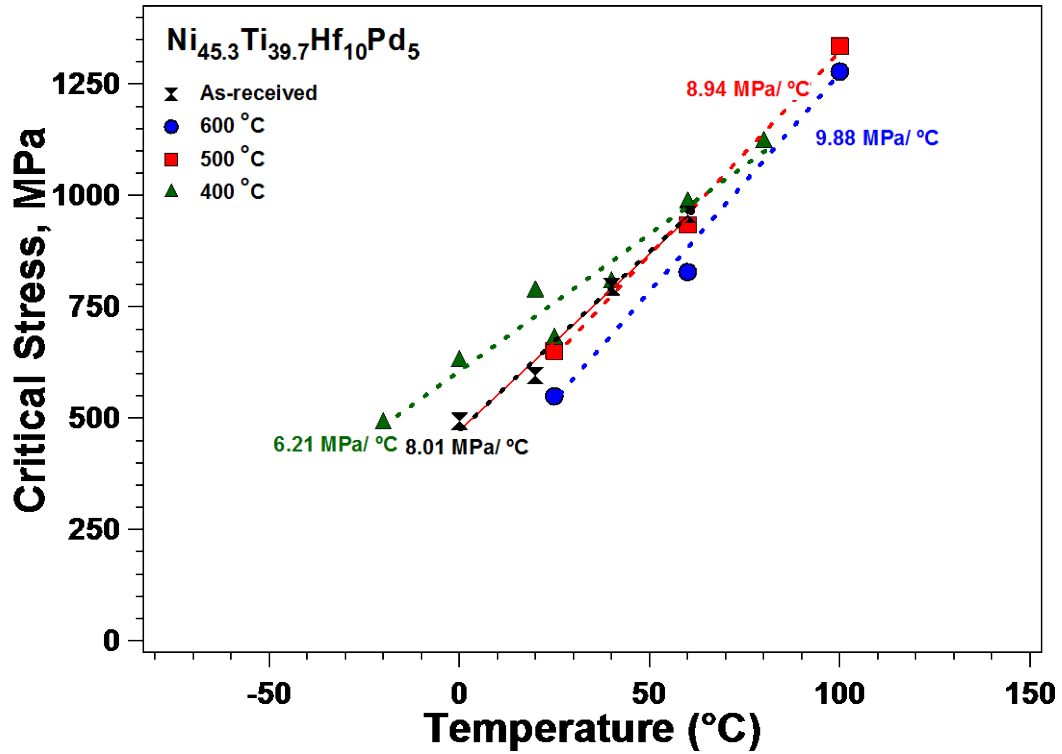
Figure 5-6 Critical stress versus temperature diagram of the as-received and aged $Ni_{45.3}Ti_{39.7}Hf_{10}Pd_5$

Critical stress- temperature graph of as-received and aged $Ni_{45.3}Ti_{39.7}Hf_{10}Pd_5$ was given in Figure5.6. Critical stresses were measured by the tangent method from stress-strain curves. It is clear that critical stresses increased with temperature. This phenomenon is also known asClausius-Clapeyron relation. The C-C slopes were found to be 8.01 MPa/ºC, 6.21 MPa/ºC, 8.94 MPa/ºC and 9.88 MPa/ºC for as-received and aged samples at 400 ºC, 500 ºC and 600 ºC for 3hours, respectively. However, aging is not effective function on critical stresses, almost in all conditions, similar slopes measured.
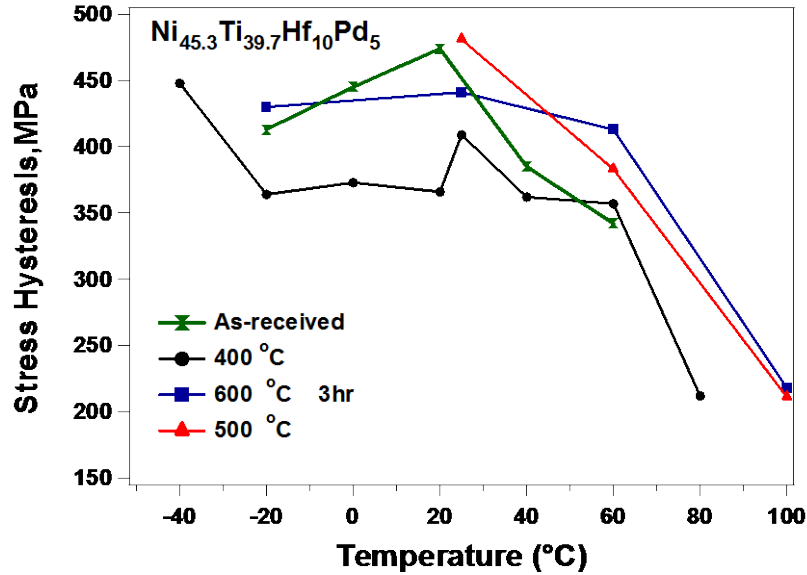
Figure 5-7 Stress hysteresis of aged $Ni_{45.3}Ti_{39.7}Hf_{10}Pd_5$

SMAs is mechanical hysteresis (stress hysteresis) which is a determinant factor for the damping applications [39]. The stress hysteresis values of $Ni_{45.3}Ti_{39.7}Hf_{10}Pd_5$ alloys as-received and aged at 400 °C, 500 °C, and 600 °C for 3 hours were given in Figure 5.7 Stress hysteresis values measured from the stress-strain graphs. They determined as the difference between the loading and unloading curves which is shown in Figure 1.4.

Stress hysteresis of 400 °C 3-h aged sample decreased when the test temperature increased from -40 to -20 °C. Next, between -20 to 60 °C temperature range hysteresis did not change as a function of test temperature. However, after 60 °C, hysteresis dropped sharply. 500 °C 3-h aged sample tested only between 25 °C to 100 °C. Hysteresis decreased as a function of temperature. Mechanical hysteresis of sample aged at 600 °C for 3 hours was almost same between -20°C to 60 °C. After that, it decreased when the test temperature increased. It is clear that stress hysteresis is highly temperature dependent.
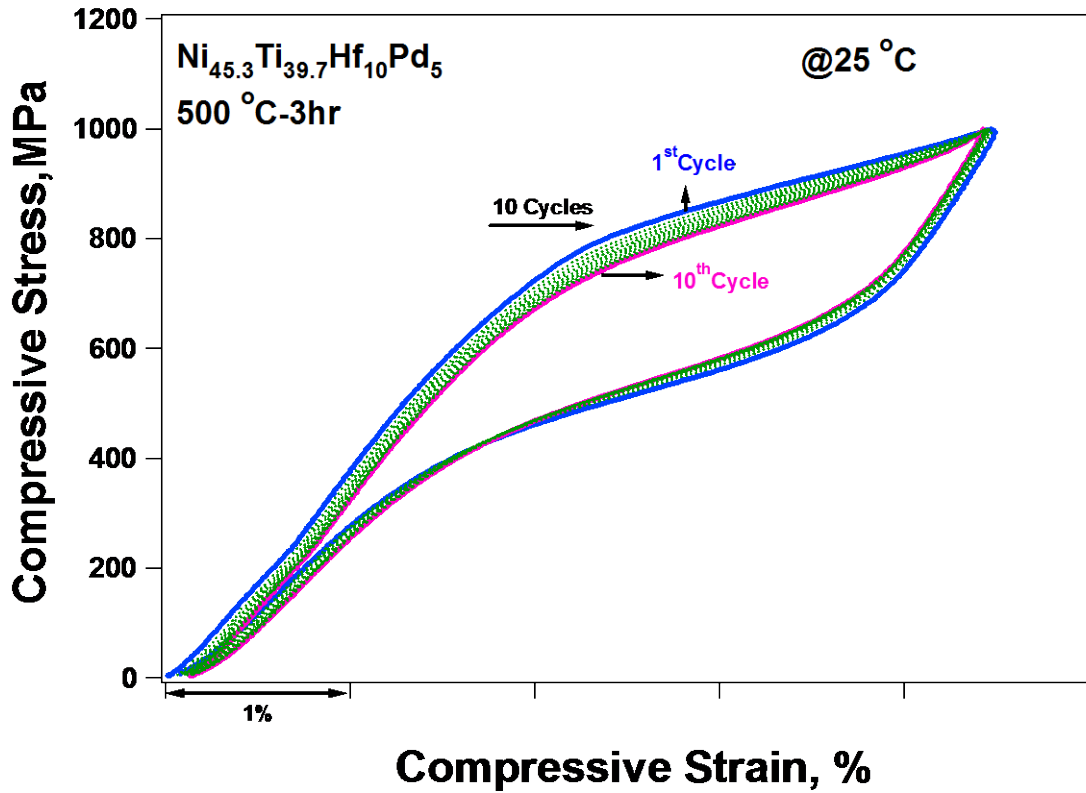
Figure 5-8 Superelastic cyclic response of aged $Ni_{45.3}Ti_{39.7}Hf_{10}Pd_5$

To invesitigate the cyclic stability, aged sample was subjectted to the cycling loading. Figure 5.8 shows the superelastic cycling of aged $Ni_{45.3}Ti_{39.7}Hf_{10}Pd_5$. Since the three aged conditions responses were similar, 500 $^{\circ}C$ 3 hours aging condition was selected for cycling test. The sample was loaded up to the strain of 4.5%, and almost full recovery was obtained with an irrecoverable strain of 0.07% in the first cycle. The sample exhibited perfect superelastic cycling behavior with an irrecoverable strain of 0.208% in 10th cycling.

5.4   Thermal Cycling Under Constant Stress Responses

Temperature cycling under constant stress level tests has been carried out for aged $Ni_{45.3}Ti_{39.7}Hf_{10}Pd_5$ alloy. Each sample thermally cycled under selected high-stress level in austenite phase than cooled to down to below M_f to fully transform and heated up again

above A_f temperature to transform to the austenite phase. With the thermal cycling recoverable, irrecoverable strains and M_s temperatures were determined by high-stress level. M_s temperatures measured from 800 MPa curves and they were found to be 16 °C, 33 °C, and 29 °C aged at 400 °C, 500 °C, and 600 °C for 3 hours samples. Recoverable and irrecoverable strains were also determined to be 2.44, 3%, 2.77% and 0.56, 0.66, 0.76% for aged at 400 °C, 500 °C, and 600 °C-3h samples, respectively under 800 MPa. The irrecoverable strains increased with the increasing aging temperatures.
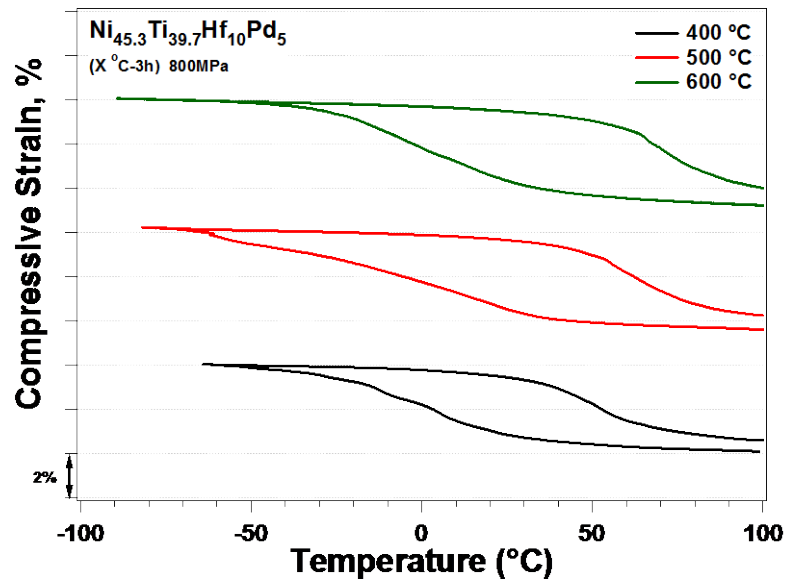
Figure 5-9 The constant stress, strain-temperature responses of aged $Ni_{45.3}Ti_{39.7}Hf_{10}Pd_5$samples at 800 MPa
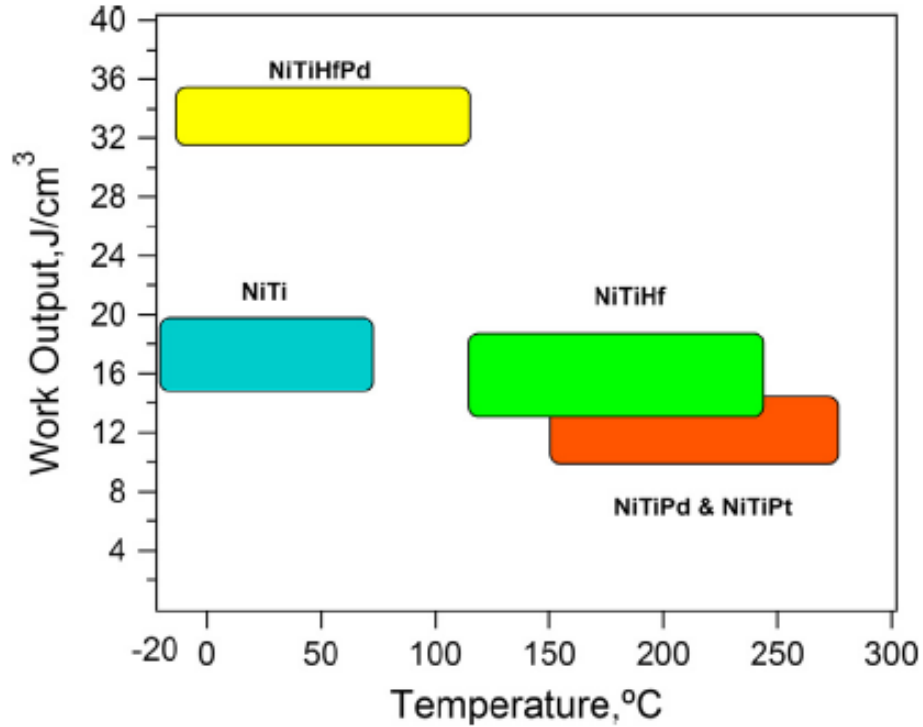
Figure 5-10. Comparison of the work output energy densities for NiTi-based shape memory alloys as a function of operation temperature [4]

Work output of SMA should be mentioned since it is an important measurement for the solid-state actuator. Work output is related to applied stress and transformation strain. Mathematically, work output can be calculated by multiplying of recoverable strain and applied stress. Higher work output decreases the required weight and volume. Thus, work output capacity can be expressed as the efficiency of SMAs [4]. Figure 5-10 shows a comparison of the work output densities for NiTi-based SMAs. NiTiHfPd alloys exhibit the highest work output densities between 32-36 J/cm3. In previous study, work output capacity of as-received $Ni_{45.3}Ti_{39.7}Hf_{10}Pd_5$ was found to be 29 J/cm^3 and J 25 J/cm^3 at 700 and 1000 MPa, respectively [32]. The work output density decreased as increasing stress level due to the lower recoverable strain. Shape memory properties of aged $Ni_{45.3}Ti_{39.7}Hf_{10}Pd_5$ alloy under 800MPa were given in table 5.1. It was found to be the

work output of this alloy 19.52, 24 and 22.16 J/cm^3 for aged at 400 $^{\text{o}}$C-3hr, 500 $^{\text{o}}$C-3hr, 600 $^{\text{o}}$C-3hr, respectively.

Table 5.1. Comparison of shape memory parameters of aged NiTiHfPd alloy under 800 MPa

Aging Temp (ºC)	M_S (ºC)	Total Strain, %	Irrecoverable Strain, %	Work Output J/cm^3
400 ºC-3hr	16	3	0.56	19.52
500 ºC-3hr	33	3.66	0.66	24
600 ºC-3hr	29	3.53	0.76	22.16

5.5 The superelastic behavior of NiTiHfPd alloys under selected loading rates

Last two decades, SMAs have been under investigation for many applications, one of them is civil structures because of their unique behavior [40]. While shape memory effect is shown by heating and superelasticity is taken place by releasing the load [41]. Higher damping capacity and larger recoverable strain are obtained from the shape memory then superelasticity, however, heating- cooling cycle is slower than the stress-strain cycle. Thus, in many studies, researcher have been focused on the superelastic behavior of SMAs rather than shape memory effect [41].

Beside the damping capacity, SMAs exhibit high fatigue and corrosion resistance which make them a useful candidate for civil structures. They can be used as connector or damping elements for bridges structures [40, 42].

In the light of this information, we investigated the effect of loading frequency and temperature on the superelastic responses of single and polycrystalline NiTiHfPd alloys. Tests were employed at different strain amplitude, various temperatures and loading

frequencies from 0.05 Hz to 1 Hz. Any transformation was not observed till -60 °C and based on the previous study, it was assumed A_f is lower than -60 °C. Thus, all the samples performed above A_f temperatures.

In dynamic application, SMAs are exposed to high loading rates. In this purpose, NiTiHfPd alloys are examined under different loading rate. Figure 5.9 shows the stress-strain response of $Ni_{45.}Ti_{39.7}Hf_{10}Pd_5$ aged at 400 °C-3hr alloys. The sample was loaded up to 5 % at each frequency and test temperatures. It is clear from the curves that loading rate does not affect the forward transformation, however, in the backward transformation, 0.05Hz loading rate was separated from the others, and it absorbed higher energy.
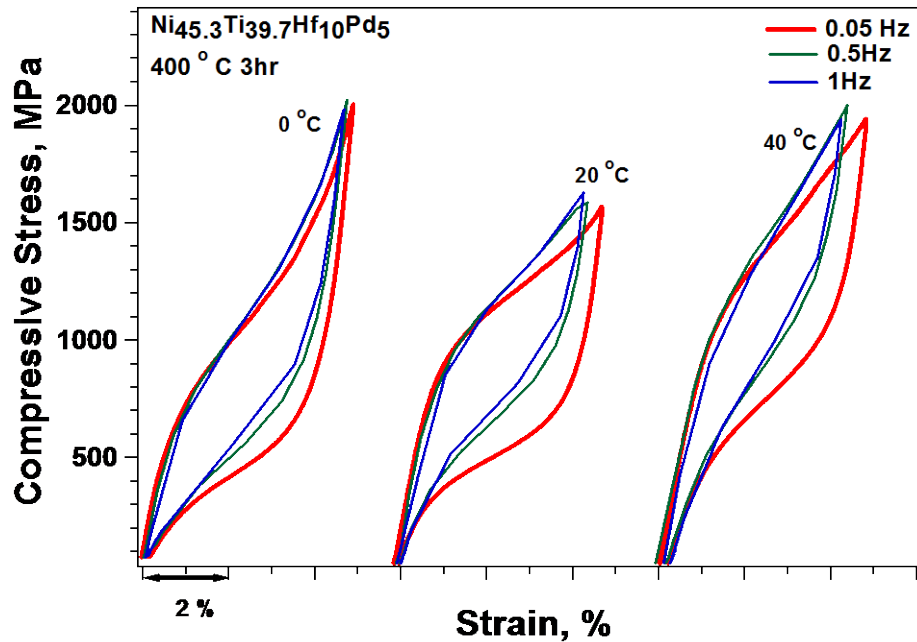

Figure 5-11 Experimental stress-strain curves of aged polycrystalline $Ni_{45.}Ti_{39.7}Hf_{10}Pd_5$ alloys at various temperatures with different strain rate
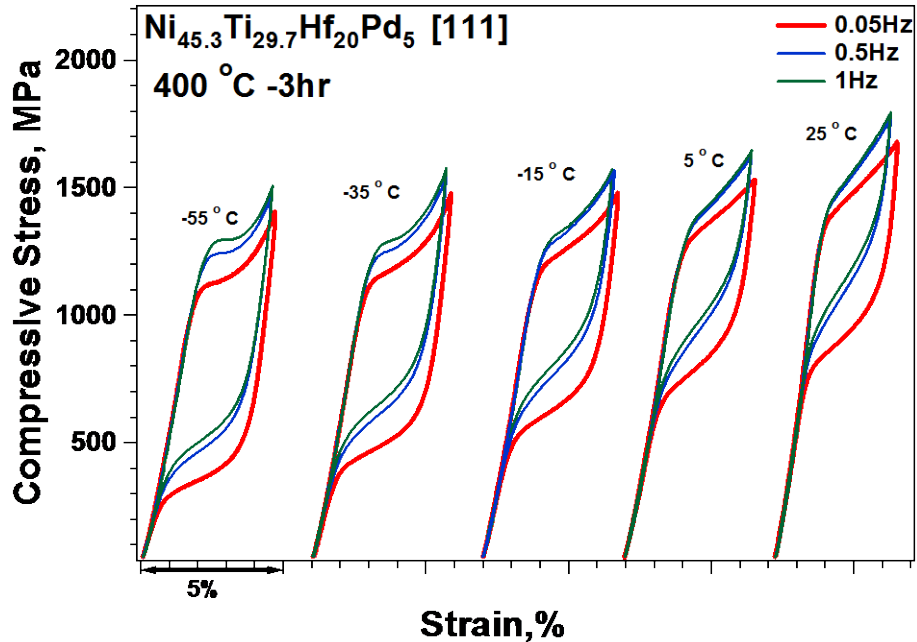
Figure 5-12 Experimental stress-strain curves of aged $Ni_{45.}Ti_{29.7}Hf_{20}Pd_5$ [111] orientation alloy at various temperatures with different strain rate

Figure 5.10 shows that compression behavior of $Ni_{45.}Ti_{29.7}Hf_{20}Pd_5$ [111] orientation alloy at different frequencies and various temperatures. It was clear that the curves at 0.5 Hz and 1 Hz lap to each other. While the forward transformation was similar for all the frequencies, in the backward transformation, 0.05 Hz curves were separated from others. The sample was transformed at lower critical stress at 0.05 Hz when it was compared with 0.5 Hz and 1Hz frequencies. Between -55 °C and -15 °C visible plateau region was observed, after -15 °C plateau was disappeared. The sample was showed perfect superelasticity at all the test temperatures and frequencies; irrecoverable strain was not observed.

The absorbed energy was calculated from the highest stress level of each temperature. The area of under the stress-strain curves (stress hysteresis area) provides the dissipated energy/damping capacity. Figure 5.11 (a) shows the absorbed energy of

$Ni_{45.3}Ti_{39.7}Ti_{10}Pd_5$ aged at 400 °C for 3 hours. The absorbed energy was found to be 25.13, 20.8 and 17.71 J/mm^3 at 0°C, 20 °C and 40 °C for 0.05Hz, 0.5Hz, 1Hz frequencies, respectively. It is clear that higher strain rate resulted in lower absorbed energy. In contrast, absorbed energies did not change as a function of test temperatures.

Absorbed energy versus temperature graph of $Ni_{45.3}Ti_{29.7}Ti_{20}Pd_5$ [111] was given in Figure 5.3-(b). The sample was tested in the wider temperature range from -55 °C to 25 °C. The same trend was observed in $Ni_{45.3}Ti_{29.7}Ti_{20}Pd_5$ [111] alloy. Higher frequencies resulted in lower dissipated energies. Above 35 °C, dissipated energy decreased linearly up to 5 °C then it saturated. Acar et al [43] have been worked on polycrystalline $Ni_{45.3}Ti_{29.7}Ti_{20}Pd_5$ and they also observed the similar trend. Dissipated energy at the high frequency is lower.
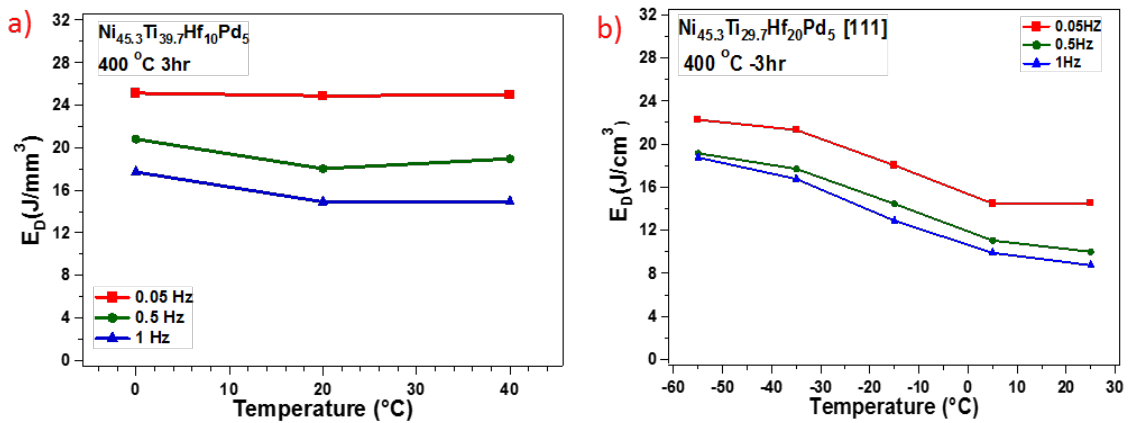

Figure 5-13 Absorbed the energy of a) $Ni_{45.3}Ti_{39.7}Ti_{10}Pd_5$ b) $Ni_{45.3}Ti_{29.7}Ti_{20}Pd_5$ aged at 400 °C-3hr samples as a function of test temperatures.
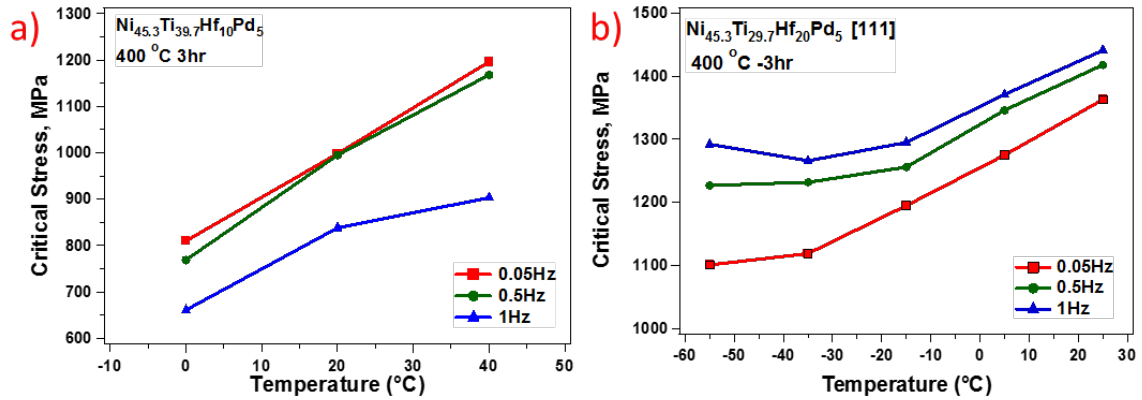
Figure 5-14 Critical stresses of a) $Ni_{45.3}Ti_{39.7}Ti_{10}Pd_5$ b) a) $Ni_{45.3}Ti_{29.7}Ti_{20}Pd_5$ aged at 400 °C-3hr samples as a function of test temperatures.

Temperature has a significant effect on the mechanical behavior of the materials. Under compression, the mechanical behavior can be altered with testing temperature. In SMAs, critical stress represents the stress-induced martensitic transformation under loading. One can see that critical stress increased while the test temperature increased. Also, critical stress for strain rate shows different values. While the critical stress for 1 Hz frequency in $Ni_{45.3}Ti_{39.7}Ti_{10}Pd_5$ found to be the lowest, critical stress for 1 Hz frequency in [111] $Ni_{45.3}Ti_{29.7}Ti_{20}Pd_5$ alloy had the highest values.

5.6   Summary

In this chapter, $Ni_{45.3}Ti_{39.7}Hf_{10}Pd_5$ and $Ni_{45.3}Ti_{29.7}Hf_{20}Pd_5$ alloys were investigated. Shape memory behavior of high temperature polycrystalline $Ni_{45.3}Ti_{29.7}Hf_{20}Pd_5$ alloy was examined. Another polycrystalline $Ni_{45.3}Ti_{39.7}Hf_{10}Pd_5$ alloy was aged at selected temperatures and their temperature-dependent superelastic behavior was revealed. At the final study in this chapter is strain rate test to reveal the damping capacity of [111] orientation $Ni_{45.3}Ti_{29.7}Hf_{20}Pd_5$ and polycrystalline $Ni_{45.3}Ti_{39.7}Hf_{10}Pd_5$ alloys. The significant results have been summarized,

1. It was found that transformation temperatures of polycrystalline of $Ni_{45.3}Ti_{29.7}Hf_{20}Pd_5$ highly dependent on aging temperatures. Thus, they can be operated in the wider range of temperatures between 25 °C-250 °C.

2. The temperature-dependent superelastic behavior of aged $Ni_{45.3}Ti_{39.7}Hf_{10}Pd_5$ samples was investigated. It was found to be aging was not a strong function for the $Ni_{45.3}Ti_{39.7}Hf_{10}Pd_5$ alloy. They showed similar superelastic responses at all aging temperatures.

3. They showed perfect superelastic behavior up to the strain of 5% at 25 °C for all aging condition.

4. C-C relation of the aged samples of $Ni_{45.3}Ti_{39.7}Hf_{10}Pd_5$ alloy was very similar to each other, and they were found to be 6.11 MPa/ °C, 8.94 MPa/ °C, and 6.95 MPa/ °C after aging at 400 °C, 500 °C and 600 °C for 3hr, respectively.

5. Work output densities of $Ni_{45.3}Ti_{39.7}Hf_{10}Pd_5$ alloy were found to be 19.52, 24 and 22.16 J/cm^3 for aged at 400 °C-3hr, 500 °C-3hr, 600 °C-3hr, respectively.

6. While the polycrystalline $Ni_{45.3}Ti_{39.7}Hf_{10}Pd_5$ alloy aged at 400 °C for 3hr exhibits 25-16 J.cm^{-3} damping capacity, 400 °C-3hr aged [111]-orientated $Ni_{45.3}Ti_{29.7}Hf_{20}Pd_5$ shows 10 to 23 J.cm^{-3} damping capacity.

7. Critical stress was affected by both temperature and strain rate. Critical stress increased as a function of temperature for both alloys.

6. Chapter Six: Conclusion

In this study, shape memory properties, microstructure and mechanical behavior of $Ni_{40.3}Ti_{34}Hf_{20}Pd_5$, $Ni_{40.3}Ti_{39.7}Hf_{15}Pd_5$, $Ni_{40.3}Ti_{44.7}Hf_{10}Pd_5$, and $Ni_{45.3}Ti_{29.7}Hf_{20}Pd_5$, $Ni_{45.3}Ti_{39.7}Hf_{10}Pd_5$ alloys were investigated. Hf contains were varied from 20 to 10 at% and Pd was 5 at %.

At first, composition effects were detailed of $Ni_{40.3}Ti_{34}Hf_{20}Pd_5$, $Ni_{40.3}Ti_{39.7}Hf_{15}Pd_5$, and $Ni_{40.3}Ti_{44.7}Hf_{10}Pd_5$. It was founded that Hf contents have significant effects on the microstructure, transformation temperatures, and mechanical behavior. When the Hf content increases, transformation temperatures increase, shape memory properties (strain hysteresis, superelastic responses) weaken. The highest transformation strain was obtained for the $Ni_{40.3}Ti_{44.7}Hf_{10}Pd_5$. However, $Ni_{40.3}Ti_{34}Hf_{20}Pd_5$, $Ni_{40.3}Ti_{39.7}Hf_{15}Pd_5$ alloys showed higher TTs (up to 250 ^{o}C) and strength at high stress-level than the $Ni_{40.3}Ti_{44.7}Hf_{10}Pd_5$ alloy. Additionally, they have narrow hysteresis at the high-stress level, and these properties make them a bright candidate for the high temperatures and actuators applications.

Besides the composition effects, a comprehensive aging study was conducted on the $Ni_{40.3}Ti_{34}Hf_{20}Pd_5$, $Ni_{40.3}Ti_{39.7}Hf_{15}Pd_5$, $Ni_{40.3}Ti_{44.7}Hf_{10}Pd_5$, and $Ni_{45.3}Ti_{29.7}Hf_{20}Pd_5$ alloys. It was found that aging is a powerful method to adjust the transformation temperatures of SMAs. With the aid of heat treatments, TTs raised from room temperatures to around 250 ^{o}C. However, aging was not affected by the shape memory effect of the $Ni_{40.3}Ti_{34}Hf_{20}Pd_5$, $Ni_{40.3}Ti_{39.7}Hf_{15}Pd_5$, and $Ni_{40.3}Ti_{44.7}Hf_{10}Pd_5$ because of the presence and formation of secondary phases. Although aged 350 ^{o}C-3hr aged $Ni_{40.3}Ti_{44.7}Hf_{10}Pd_5$ alloy showed relatively wider shape memory effect, it did not show promising superelastic responses.

Another systematic study was conducted on the 400 $^{\circ}$C-3 hr aged $Ni_{45.3}Ti_{39.7}Hf_{10}Pd$ polycrystalline alloys and [111] orientated $Ni_{45.3}Ti_{29.7}Hf_{20}Pd_5$ single crystals. Samples were subjected to the different strain rates and the damping capacities were found to be 16-25 $J.cm^{-3}$ and 10-23 $J.cm^{-3}$ for $Ni_{45.3}Ti_{39.7}Hf_{10}Pd_5$ and [111] oriented $Ni_{45.3}Ti_{29.7}Hf_{20}Pd_5$, respectively.

References

1. Dimitris, C.L., *Shape memory alloys: Modeling and engineering applications*. 2008, Springer.
2. Rao, A., A.R. Srinivasa, and J.N. Reddy, *Design of shape memory alloy (SMA) actuators*. Vol. 3. 2015: Springer.
3. Volume, A.H., *2: Properties and Selection: Nonferrous Alloys and Special-Purpose Materials.* ASM international, 1990: p. 889-896.
4. Acar, E., *Precipitation, orientation and composition effects on the shape memory properties of high strength NiTiHfPd alloys.* 2014.
5. Saedi, S., et al., *Thermomechanical characterization of Ni-rich NiTi fabricated by selective laser melting.* Smart Materials and Structures, 2016. **25**(3): p. 035005.
6. Van Humbeeck, J., *Damping capacity of thermoelastic martensite in shape memory alloys.* Journal of Alloys and Compounds, 2003. **355**(1): p. 58-64.
7. Mehrabi, K., et al., *Influence of chemical composition and manufacturing conditions on properties of NiTi shape memory alloys.* Materials Science and Engineering: A, 2008. **481**: p. 693-696.
8. Arciniegas, M., et al., *Study of hardness and wear behaviour of NiTi shape memory alloys.* Journal of Alloys and Compounds, 2008. **460**(1): p. 213-219.
9. Saedi, S., et al., *The influence of heat treatment on the thermomechanical response of Ni-rich NiTi alloys manufactured by selective laser melting.* Journal of Alloys and Compounds, 2016. **677**: p. 204-210.
10. Han, X., et al., *In situ observations of the reverse martensitic transformations in a TiNiHf high temperature shape memory alloy.* Materials Letters, 1997. **30**(1): p. 23-28.
11. Saghaian, S., et al., *Tensile shape memory behavior of Ni 50.3 Ti 29.7 Hf 20 high temperature shape memory alloys.* Materials & Design, 2016. **101**: p. 340-345.
12. Ma, J., I. Karaman, and R.D. Noebe, *High temperature shape memory alloys.* International Materials Reviews, 2010. **55**(5): p. 257-315.
13. Evirgen, A., et al., *Microstructural characterization and superelastic response of a Ni 50.3 Ti 29.7 Zr 20 high-temperature shape memory alloy.* Scripta Materialia, 2014. **81**: p. 12-15.
14. Patriarca, L., et al., *High temperature shape memory behavior of Ni 50.3 Ti 25 Hf 24.7 single crystals.* Scripta Materialia, 2016. **115**: p. 133-136.
15. Jani, J.M., et al., *A review of shape memory alloy research, applications and opportunities.* Materials & Design, 2014. **56**: p. 1078-1113.
16. Barbarino, S., et al., *A review on shape memory alloys with applications to morphing aircraft.* Smart Materials and Structures, 2014. **23**(6): p. 063001.
17. Saedi, S., *Shape Memory Behavior of Dense and Porous NiTi Alloys Fabricated by Selective Laser Melting.* 2017.
18. Elahinia, M., *Shape memory alloy actuators: design, fabrication and experimental evaluation*. 2015: John Wiley & Sons.

19.   Sehitoglu, H., et al., *Compressive response of NiTi single crystals.* Acta Materialia, 2000. **48**(13): p. 3311-3326.

20.   Gall, K., et al., *Effect of microstructure on the fatigue of hot-rolled and cold-drawn NiTi shape memory alloys.* Materials Science and Engineering: A, 2008. **486**(1): p. 389-403.

21.   Gall, K. and H. Maier, *Cyclic deformation mechanisms in precipitated NiTi shape memory alloys.* Acta Materialia, 2002. **50**(18): p. 4643-4657.

22.   Kaya, I., et al., *Effects of aging on the shape memory and superelasticity behavior of ultr a-high strength Ni54Ti46 alloys under compression.* Materials Science & Engineering A, 2016. **678**: p. 93-100.

23.   Zheng, Y., et al., *Effect of ageing treatment on the transformation behaviour of Ti–50.9 at.% Ni alloy.* Acta Materialia, 2008. **56**(4): p. 736-745.

24.   Zhou, Y., et al., *Origin of 2-stage R-phase transformation in low-temperature aged Ni-rich Ti–Ni alloys.* Acta materialia, 2005. **53**(20): p. 5365-5377.

25.   Otsuka, K. and X. Ren, *Physical metallurgy of Ti–Ni-based shape memory alloys.* Progress in materials science, 2005. **50**(5): p. 511-678.

26.   Yoneyama, T. and S. Miyazaki, *Shape memory alloys for biomedical applications*. 2008: Elsevier.

27.   Karaca, H., et al., *Shape memory behavior of high strength Ni 54 Ti 46 alloys.* Materials Science and Engineering: A, 2013. **580**: p. 66-70.

28.   Kaya, I., *Shape memory and transformation behavior of high strength 60NiTi in compression.* Smart Materials and Structures, 2016. **25**(12): p. 125031.

29.   Saedi, S., et al., *Structural Vibration Control Using High Strength and Damping Capacity Shape Memory Alloys*, in *Dynamics of Civil Structures, Volume 2*. 2017, Springer. p. 259-266.

30.   Schwartz, M., *New materials, processes, and methods technology*. 2005: CRC Press.

31.   Hong, S.H., et al., *Influence of Zr content on phase formation, transition and mechanical behavior of Ni-Ti-Hf-Zr high temperature shape memory alloys.* Journal of Alloys and Compounds, 2017. **692**: p. 77-85.

32.   Acar, E., et al., *Compressive response of Ni45. 3Ti34. 7Hf15Pd5 and Ni45. 3Ti29. 7Hf20Pd5 shape-memory alloys.* Journal of materials science, 2015. **50**(4): p. 1924-1934.

33.   Pasko, A., et al. *Glass forming ability and thermodynamic properties of Ti (Zr, Hf) NiCu shape memory alloys*. in *Journal de Physique IV (Proceedings)*. 2003. EDP sciences.

34.   Liang, X., et al., *Thermal cycling stability and two-way shape memory effect of Ni–Cu–Ti–Hf alloys.* Solid state communications, 2001. **119**(6): p. 381-385.

35.   Karaca, H., et al., *Microstructure and transformation related behaviors of a Ni 45.3 Ti 29.7 Hf 20 Cu 5 high temperature shape memory alloy.* Materials Science and Engineering: A, 2015. **627**: p. 82-94.

36.   Kim, H.Y., et al., *Cold workability and shape memory properties of novel Ti–Ni–Hf–Nb high-temperature shape memory alloys.* Scripta Materialia, 2011. **65**(9): p. 846-849.

37. Karaca, H., et al., *Shape memory behavior of high strength NiTiHfPd polycrystalline alloys.* Acta Materialia, 2013. **61**(13): p. 5036-5049.

38. Delville, R., et al., *Transmission electron microscopy study of phase compatibility in low hysteresis shape memory alloys.* Philosophical magazine, 2010. **90**(1-4): p. 177-195.

39. Turabi, A.S., et al., *Experimental Characterization of Shape Memory Alloys.* Shape Memory Alloy Actuators: Design, Fabrication, and Experimental Evaluation, 2015: p. 239-277.

40. Ozbulut, O.E., S. Hurlebaus, and R. Desroches, *Seismic Response Control Using Shape Memory Alloys: A Review.* Journal of Intelligent Material Systems and Structures, 2011. **22**(14): p. 1531-1549.

41. Pan, Q. and C. Cho, *The investigation of a shape memory alloy micro-damper for MEMS applications.* Sensors, 2007. **7**(9): p. 1887-1900.

42. Song, G., N. Ma, and H.-N. Li, *Applications of shape memory alloys in civil structures.* Engineering structures, 2006. **28**(9): p. 1266-1274.

43. Acar, E., O.E. Ozbulut, and H.E. Karaca, *Experimental investigation and modeling of the loading rate and temperature dependent superelastic response of a high performance shape-memory alloy.* Smart Materials and Structures, 2015. **24**(7): p. 075020.

VITA

Guher Pelin Toker was graduated from Suleyman Demirel University, Turkey, as a Mechanical Engineer in 2012. Then, she received Master of Science degree in Mechanical Engineering of Erciyes University in 2014. In 2016, she started her M.Sc. study in the Department of Mechanical Engineering at the University of Kentucky. During the M.Sc. study, she worked under Prof. Haluk E. Karaca and she focused on the shape memory properties of high strength shape memory alloys.